Kinetic Studies of Radical Reactions using time-resolved EPR

Inaguaraldissertation

zur

Erlangung der Würde eines Doktors der Philosophie

vorgelegt der

Philosophish-Naturwissenschaftlichen Fakultät

der Universität Basel

von

Daniela Hristova

aus Bobov dol (Bulgaria)

Basel, 2005

Kinetic Studies of Radical Reactions using time-resolved EPR

Inaguaraldissertation

zur

Erlangung der Würde eines Doktors der Philosophie

vorgelegt der

Philosophish-Naturwissenschaftlichen Fakultät

der Universität Basel

von

Daniela Hristova

aus Bobov dol (Bulgaria)

Basel, 2005

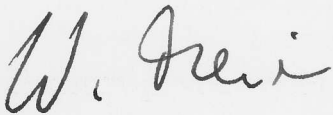Genehmigt von der Philosophisch-Naturwissenschaftlichen Fakultät auf Antrag der

Herren

Prof. Dr. Wolfgang Meier   Prof. Dr. Georg Gescheidt

(Referent)   (Korreferent)

Basel, 28 Februar 2005

Prof. Dr. Jakob Wirz

Dekan

Contents

Chapter 1

Introduction

Over the past decades, the impact of new developments in the field of radical polymerization on the synthetic possibilities in macromolecular design has been unprecedented. Free radical polymerization is a very rapidly developing field particularly because of its commercial importance, facile reaction conditions and synthetic manipulations, which are much easier than in anionic or carbocationic systems. It combines the advantages like the ability to use a large range of monomers which can be polymerized and undemanding reaction conditions, including monomer purification, residual water, wide temperature range, and the use of bulk systems.

Radicals can be generated efficiently and under controlled conditions by photolytic α-cleavage of a suitable photoinitiator. Therefore, significant efforts have been devoted to the development of new photoinitiators for UV and visible curing technology. Upon absorption of a photon of suitable wavelength, photoinitiators undergo homolytic bond cleavage to produce two identical or two different reactive radicals which are able to add to the double bond of the monomer and initiate polymerization.

Understanding the free radical polymerization process should lead to more efficient polymer production, saving both time and money.

Time-resolved optical spectroscopy is the most popular technique for determination the rates of radical reactions in solution. The optical absorption of the radicals generated and of the species formed subsequently can be followed in the UV/Vis spectra. This, however is only feasible, if the reactant and product radicals absorb sufficiently - which often is not the case. It has been demonstrated that time-resolved infrared spectroscopy is another tech-

nique, which may be applied as a selective tool for kinetic studies of radicals with well-resolved vibrational absorption.

The disadvantage of all optical methods is that the radicals under investigation should possess well-defined absorptions. In addition, overlapping optical absorptions of the initiator molecules and the radicals may occur and cause the kinetic analysis of the transient to be problematic.

The technique of time-resolved Electron Paramagnetic Resonance (TR-EPR) has recently become the method of choice for obtaining addition rate constants (k_{add}) in free radical polymerization systems. TR-EPR spectroscopy has advantages over the optical spectroscopy not only in terms of the identification of short lived radicals but also gives structural and dynamic information on these species and some insight in the study of their properties.

Additional insights are possible by the application of state-of-the-art theoretical methods. Here calculations on appropriate levels of theory are utilized to rationalize experimental observations and, partly, to predict molecular properties.

The following chapters present several aspects of photoinitiated polymerization processes. First, the efficiency of photoinitiators in terms of rate constants are discussed. Then the reactivity in dependence of environmental effects, eg. viscosity or reactivity with oxygen is reported. Some light will be shed on photophysical behavior of formulations containing photoinitiators. Finally, the theoretical background of TR-EPR is summarized.

Chapter 8

Summary

The presented work has demonstrated, that TR-EPR is a powerful tool for the determination of the decisive structural and kinetic parameters for the evaluation of photoinitiator efficiency. Additional insights are provided by the application of theoretical calculations. This combination of experimental and theoretical methodology provides a basis for the design and development of innovative phototriggers.

On the bases of the results presented in this thesis we can make the following conclusions:

- TR-EPR allows the determination of addition rate constants in the cases where optical spectroscopy doesn't have sufficient resolution as well as provides structural information of the reactive species.

- Phosphinoyl radicals generated by photolysis of acyl and bis(acyl)phosphine oxides, possess high rate constants of addition to n-butyl acrylate, HDDA, styrene and 1-vynil-2-pyrrolidon. Analysis of the spin population at the phosphorus atom supports the experimental observations of TR-EPR spectra that greater localization of the spin population at the phosphorus atom results in faster rates of addition.

- A series of substituted benzoyl radicals have been generated by laser flash photolysis of α-amino ketones and bis(acyl)phosphine oxides. The benzoyl radicals were characterized by time-resolved EPR in toluene solution and their absolute rate constants for addition to n-butyl acrylate were determined. The experiments demonstrate two concentration domains of reactivity. The reactivity of benzoyl radicals decreases at high viscosity.

- Benzoyl radicals react faster with oxygen than phosphinoyl radicals, therefore, they can be used as oxygen scavenges.

- The fluorescence properties of the photoinitiators can be used to increase the in depth cure of the formulation.

- DFT and *ab initio* calculations have shown to be in a good agreement with the experimental data.

to my parents
and Gergana

Acknowledgments

Any project no matter how individual will almost certainly require input, assistance or encouragement from others, my thesis is no exception.

I owe an immense debt of gratitude to my supervisor, **Prof. Dr. Georg Gescheidt** for giving me the opportunity to carry out this thesis. Ever since the first day, he has been a constant reference for me in science and how science should be. I am most grateful for his confidence, kindness and patience with me in the course of all these years. His guidance in science and his explanations from the basics have made this thesis easier. We have had a number of conversations about science and non-science related matters that I value a lot. I consider myself very lucky and most honored to have been one of his students.

I would like to thank the other member of my committee, **Prof. Dr. Wolfgang Meier** for the assistance he provided at all levels of the research project.

Special thanks to **Dr. Kurt Dietliker, Dr. Jean-Luc Bierbaum** and **Dr. Jean-Pierre Wolf**. For all I know this thesis would have never come to light without their generous support and their kindness.

My Personal thanks to **Dr. Günther Rist** and **Dr. Cornelia Palivan** for all the support and assistance they have provided me with throughout my study at the University of Basel.

I am particularly indebted to my colleague and friend **Urs Buser** who stood beside me and helped me pursue my work with determination, but also for his encouragement and care he has never failed to show me.

A very special thanks goes to **Dr. Iwo Gatlik** who first introduced me in the field of TR-EPR and patiently answered my questions.

I would also like to thank **Dr. Dmytro Neshchadin** for generously taking some time out to read an earlier version of this thesis and to offer many insightful comments and suggestions for improvement.

Special thanks also go to **Tsvetanka Stanoeva** and **Michal Respondek** for their help and encouragement.

If my professors have contributed to my intellectual formation, **Jonas**, as my best friend, has helped me to develop as a human being. Indeed, his support in times of trouble, as well as his unwavering belief in my potential as a researcher, has always been a motive for me to live up to his expectations.

Last but not least, I would like to dedicate this thesis to my parents, **Liliana** and **Kiril Hristovi** for their never-ending support and the sense of security they have given when I wanted it most. They have waited so long for this moment to come true. I am glad that their waiting has finally been rewarded.

Contents

Chapter 1

Introduction

Over the past decades, the impact of new developments in the field of radical polymerization on the synthetic possibilities in macromolecular design has been unprecedented. Free radical polymerization is a very rapidly developing field particularly because of its commercial importance, facile reaction conditions and synthetic manipulations, which are much easier than in anionic or carbocationic systems. It combines the advantages like the ability to use a large range of monomers which can be polymerized and undemanding reaction conditions, including monomer purification, residual water, wide temperature range, and the use of bulk systems.

Radicals can be generated efficiently and under controlled conditions by photolytic α-cleavage of a suitable photoinitiator. Therefore, significant efforts have been devoted to the development of new photoinitiators for UV and visible curing technology. Upon absorption of a photon of suitable wavelength, photoinitiators undergo homolytic bond cleavage to produce two identical or two different reactive radicals which are able to add to the double bond of the monomer and initiate polymerization.

Understanding the free radical polymerization process should lead to more efficient polymer production, saving both time and money.

Time-resolved optical spectroscopy is the most popular technique for determination the rates of radical reactions in solution. The optical absorption of the radicals generated and of the species formed subsequently can be followed in the UV/Vis spectra. This, however is only feasible, if the reactant and product radicals absorb sufficiently - which often is not the case. It has been demonstrated that time-resolved infrared spectroscopy is another tech-

nique, which may be applied as a selective tool for kinetic studies of radicals with well-resolved vibrational absorption.

The disadvantage of all optical methods is that the radicals under investigation should possess well-defined absorptions. In addition, overlapping optical absorptions of the initiator molecules and the radicals may occur and cause the kinetic analysis of the transient to be problematic.

The technique of time-resolved Electron Paramagnetic Resonance (TR-EPR) has recently become the method of choice for obtaining addition rate constants (k_{add}) in free radical polymerization systems. TR-EPR spectroscopy has advantages over the optical spectroscopy not only in terms of the identification of short lived radicals but also gives structural and dynamic information on these species and some insight in the study of their properties.

Additional insights are possible by the application of state-of-the-art theoretical methods. Here calculations on appropriate levels of theory are utilized to rationalize experimental observations and, partly, to predict molecular properties.

The following chapters present several aspects of photoinitiated polymerization processes. First, the efficiency of photoinitiators in terms of rate constants are discussed. Then the reactivity in dependence of environmental effects, eg. viscosity or reactivity with oxygen is reported. Some light will be shed on photophysical behavior of formulations containing photoinitiators. Finally, the theoretical background of TR-EPR is summarized.

Chapter 2

Phosphine Oxides

2.1   Introduction

Free radical polymerization forms the basis of many commercially important processes. It is preferred over other polymer synthesis methods as it shows a greater tolerance to trace amounts of impurities. Understanding the free radical polymerization process should lead to more efficient polymer production, saving both time and money, less waste and new polymer products.

UV radiation curing has become a well established technology which has found an increasing number of applications. The light-induced radical polymerization of formulations containing suitable reactive double bonds is by far the most widely used method in industry. Appropriate photoinitiators, which are key components for the success of this technology, have been available for many years. A photoinitiator is a compound, which when exposed to light, forms reactive species starting a chain reaction and inducing polymer formation.[1–3]

There are two general classes of photoinitiators (Figure 2.1):

- Those that undergo direct photofragmentation on exposure to UV or visible light and produce active free radical intermediates.

- Those that can abstract a hydrogen from a suitable hydrogen donor followed by electron transfer to form a free radical species.
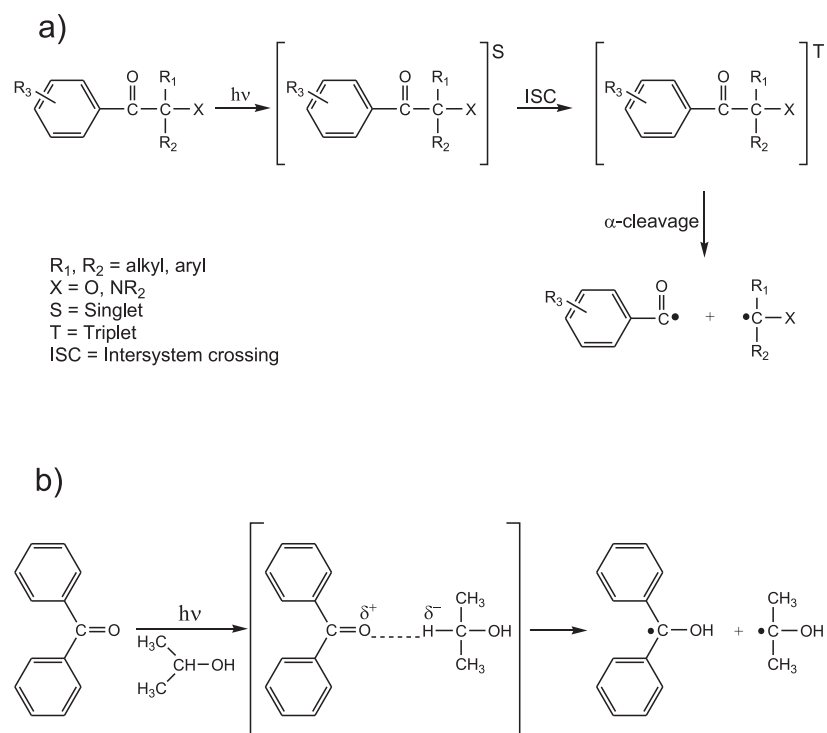
Figure 2.1: a) Photolytic α-Cleavage of alkylaryl ketones b) Photoreduction of benzophenone by isopropanol.

The optimum use of photocurable adhesives can be best achieved once the basis for their unique properties is properly addressed. This primarily requires a detailed knowledge of the kinetics of the curing process, of the mechanical properties of the cured adhesive, of the adherend's surface chemistry and morphology, and structure of the reactive species.[4–6]

The kinetic understanding of free-radical polymerization processes is of fundamental importance for efficiently generating polymeric products for a wide variety of applications.

The initiation process is the first reaction step in free-radical polymerization, leading to the generation of primary radicals. The primary radicals can be formed via a thermal decomposition processes using azo- and peroxy-type compounds, or using photoinitiators, which decompose on irradiation with UV or visible light.[7, 8]

In order to initiate the polymerization process via reaction with a monomer unit, the generated primary radicals have to leave the solvent cage that surrounds them. The ability of the primary radicals to leave the solvent cage unreacted and to start the polymerization process is quantified by the initiator efficiency f. Not all generated primary free radicals initiate polymer growth. Shortly after decomposition, the free radicals are very close to each other and recombination can occur. In addition, they can also react in an alternative way before they can react with a monomer unit (Figure 2.2). Typical values of f are between 0.5 and 0.8, depending on the viscosity of the reaction medium, indicating that the escaping process is diffusion-controlled.[9, 10]
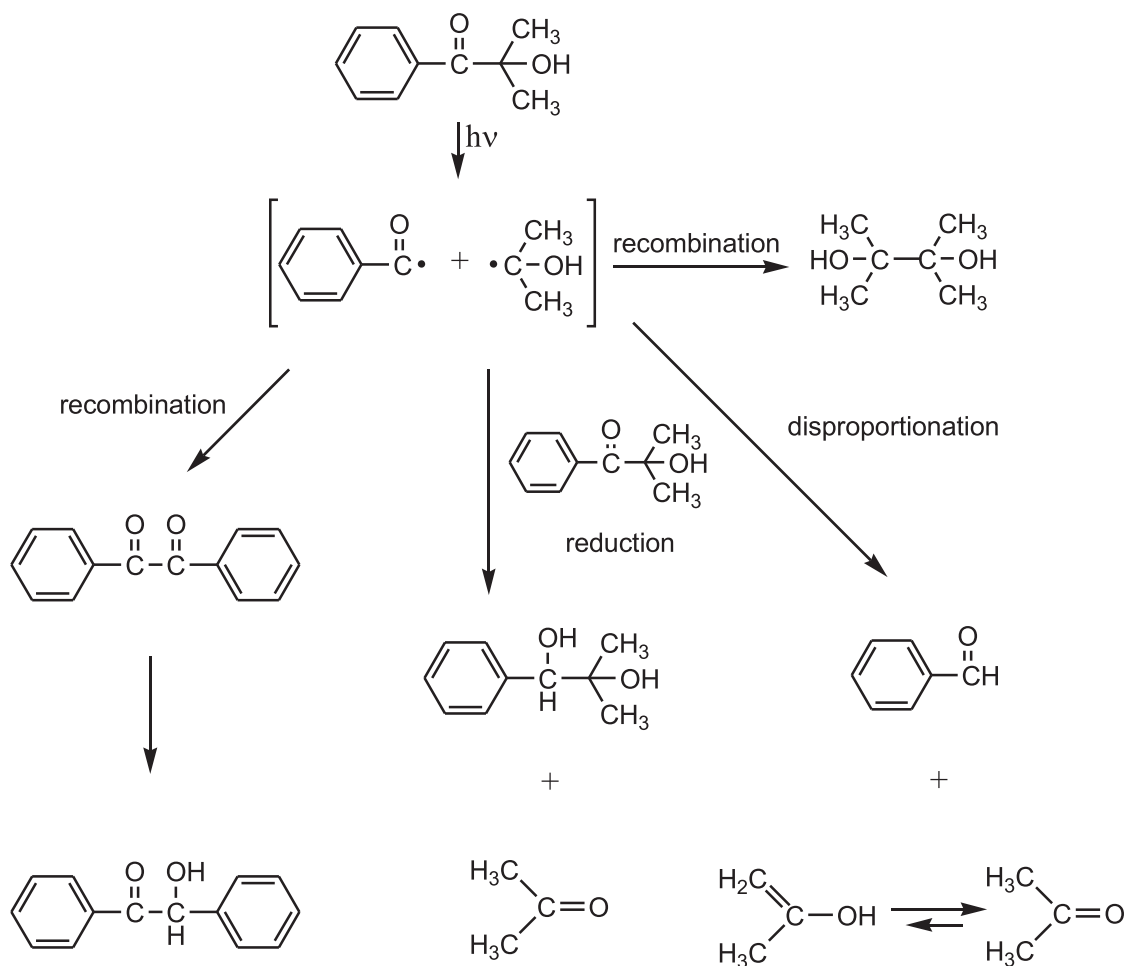

Figure 2.2: Photochemical decomposition of 1-phenyl-2-hydroxy-2-methyl-propan-1-one in solution.

The main advantage of photoinitiator use in polymerizing systems is the possibility to define exact starting- and ending points of the polymerization process by the choice of an appropriate irradiation period. In addition, the rate of (most) photoinitiator decomposition is almost independent of the reaction temperature, but depends strongly on the (UV) light intensity. An ideal photoinitiator for a specific polymerization may be defined via the following criteria:

1. The photoinitiator should decompose on irradiation with a (UV) light source. The monomer(s) used in the specific polymerization process should not absorb light at the selected wavelength.

2. The efficiency of the initiator should be high, preferably close to 1, which says that all radicals generated start a growing chain.

3. At best, there should be only one type of free-radicals species that is formed on laser irradiation.

One of the general requirements for photocurable coatings and adhesives is that the formulation is sufficiently transparent before and after setting to allow penetration of the incident radiation and to complete the cleavage of the photoinitiator. This is typically achieved by using a photoinitiator that undergoes photobleaching, i.e., a photoinitiator with decomposition products that do not absorb the curing radiation (Figure 2.3).[11, 12]
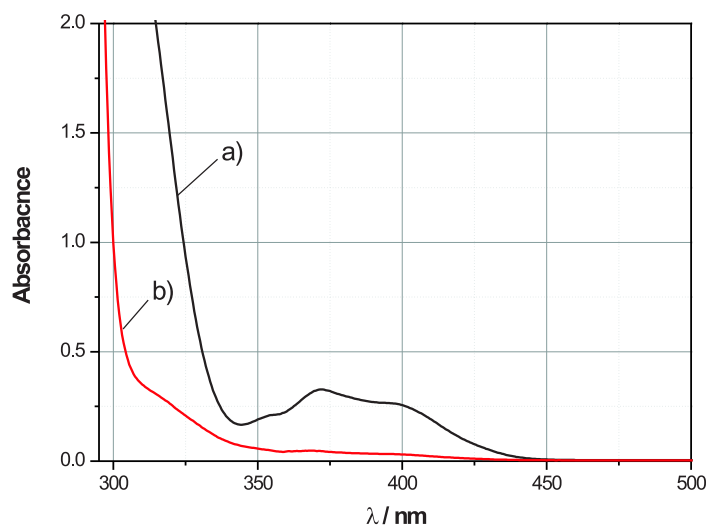
Figure 2.3: a) UV/Vis spectrum of bis(2,4,6-trimethylbenzoyl)phenylphosphine oxide before irradiation b)UV/Vis spectrum of bis(2,4,6-trimethylbenzoyl)phenylphosphine oxide before irradiation.

2.2 Compounds Investigated

2.2.1 Acylphosphine oxides

Acylphosphine oxides are high-quantum-yield photoinitiators that undergo homolytic Norrish I-type α-cleavage at the carbonyl-phosphorus bond, with generation of two free-radical species, both capable of initiating the polymerization, although with different rate constants (Figure 2.4).
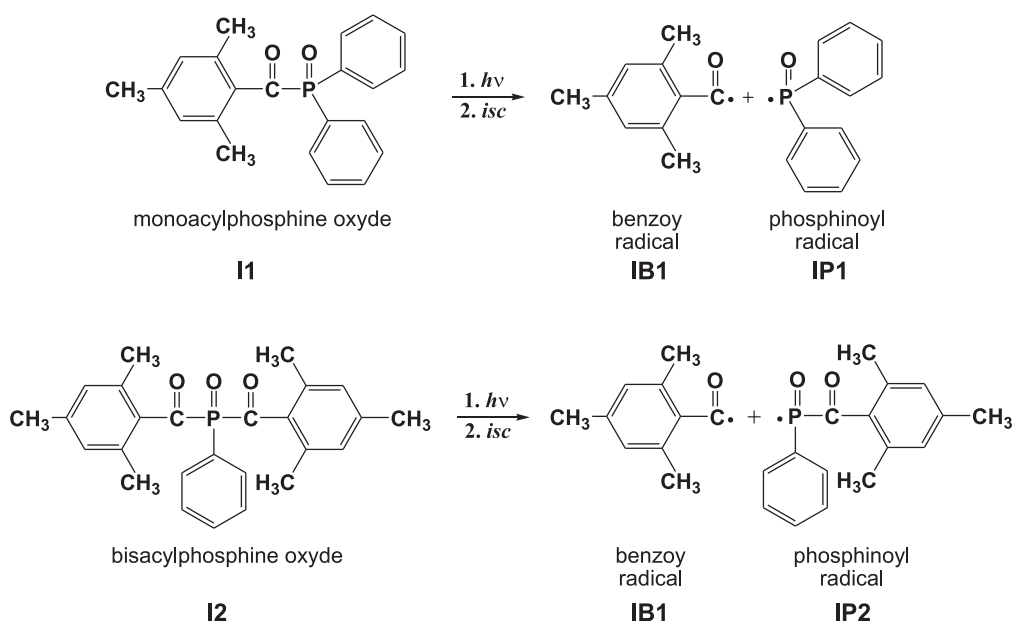
Figure 2.4: Photolytic α-Cleavage of 2,4,6-Trimethylbenzoyldiphenylphosphine oxide and bisacylphosphine oxide.

Monoacylphosphine oxide

In the production of white coatings, a high degree of whiteness is required and no yellowing of the cured film is tolerated both immediately after the curing or later as a final material.

A satisfactory radiation curing of white pigmented lacquers was first achieved using monoacylphosphine oxides as photoinitiators. These compounds have

been known for over a decade and have found use in a variety of applications. One example is 2,4,6-trimethylbenzoyl-diphenylphosphine oxide (**I1**). It is only recently that UV curable white lacquers containing these photoinitiating systems have been employed industrially, especially in furniture coatings. Another interesting feature of this photoinitiator is the possibility to cure sections of several centimeters thickness.[13–16]

Efforts have been directed to explore novel acylphosphine oxide photoinitiator structures with improved efficiency and are highly useful in applications where the use of light in the region above 400 nm is essential.[17, 18]

Bisacylphosphine oxide

Bisacylphosphine oxides are another type of structural analogs of acylphosphine oxides. The molar extinction coefficient of these compounds at 400 nm is significantly higher than that of the monoacylphosphine oxides. We have studied bis(2,4,6-trimethylbenzoyl)phenylphosphine oxide (**I2**) as an example of this type photoinitiators.

2.3   Absorption Spectra

The absorption characteristics of acylphosphine oxides differ from most other photoinitiators of the α-cleavage type in that they show enhanced absorption in the near UV/visible range. These compounds have absorption maxima around 350-380 nm, tailing to about 420 nm. Absorption spectra of **I1** and **I2** are shown in Figure 2.5.

The long wavelength absorption was identified as an n$\rightarrow\pi^*$ transition which is red-shifted as a result of a moderately strong conjugation between the phosphonyl group and the carbon atom of the adjacent carbonyl group. Further interactions may occur between a filled non-bonding orbital on the phosphonyl oxygen with the π-orbital on the same carbon atom. These effects are at a maximum when the phosphorus-oxygen bond is perpendicular to the plain determined by the aryl ring, carbonyl carbon and phosphorous.[19–22]

Bisacylphosphine oxides absorb more light in the near UV/visible spectrum. They are especially suitable for applications employing light at about 400 nm or above.
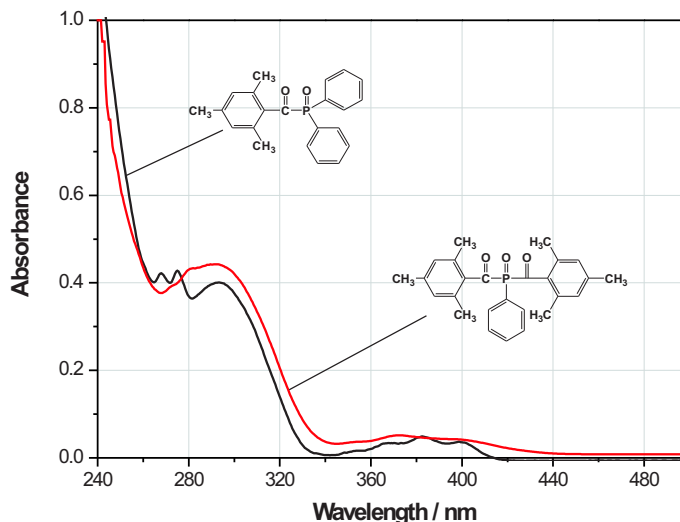
Figure 2.5: Absorption spectra of **I1** and **I2** photoinitiators in n-Hexane solution at room temperature with an optical path length d of 1 cm.

The long-wavelength absorption of acylphosphine oxides, however, is bleached after the irradiation process. Since the carbon-phosphorus bond is broken by the Norrish I type photoreaction of these compounds, interaction between the carbonyl and the phosphonyl group does not exist in the photoproducts. The resulting bleaching allows a progressively deeper penetration of the incident light into the coating layer, which enables the curing of thick layers.

2.3.1 Previous Studies

The photochemistry and photophysics of mono(acyl)phosphine oxides and bis(acyl)phosphine oxides are fairly well understood. After excitation with light, they undergo an efficient α-cleavage from the excited triplet state to produce strongly spin-polarized phosphinoyl and benzoyl radicals. Triplet states were identified by triplet quenching with naphtalene and anthracene by laser flash and steady-state photolysis. The triplet energy of these compounds has been estimated (higher than 60 kcal.mol^{-1}). Unambiguous identification of the triplet state precursor of the primary radicals was later accomplished by time-resolved EPR spectroscopy of both 2,4,6-trimethylbenzoyl-diphenylphosphine and bis(2,4,6-trimethylbenzoyl)phenylphosphine oxide.

Phosphinoyl radicals generated by photolysis of acyl and bis(acyl)phosphine oxides, possess high rate constants of addition to acrylates and related compounds. The difference in the rate constants can be explained with different degrees of radical localization and s-character on the phosphorus atom. Their reactivity is by one order of magnitude higher in comparison with the one of benzoyl radicals. Addition of halocarbons, alkenes, or oxygen reduces there lifetime. The bimolecular rate constants for quenching of phosphinoyl radicals **IP1** and **IP2** by different quenchers using laser flash photolysis are listed in Table 2.1.[23–26]

Table 2.1: Bimolecular Rate Constants for Quenching of Phosphinoyl Radicals **IP1** and **IP2** by n-Butylacrylate, Thiophenol, Bromtrichloromethane, Oxygen and Methyl Viologen in Acetonitrile Solution.

	IP1	IP2
$k_{n\text{-butylacrylate}}$ $(M^{-1}s^{-1})$	2.8×10^7	1.1×10^7
k_{PhSH_3} $(M^{-1}s^{-1})$	42×10^5	2.3×10^5
k_{BrCCl} $(M^{-1}s^{-1})$	6.9×10^8	0.9×10^8
k_{oxygen} $(M^{-1}s^{-1})$	4.2×10^9	2.7×10^9
$k_{methyl\ viologen}$ $(M^{-1}s^{-1})$	$< 10^6$	2.8×10^9

2.3.2 TR-EPR Studies

Laser flash photolysis (355 nm excitation) of diluted toluene solution of **I2** affords the TR-EPR spectrum shown in Figure 2.6. It consists of a three lines, the outer two are due to the phosphorus-centered radical **IP2** representing a phosphorus coupling $a_p = 25.8$ mT. The broad absorptive line near center field is assigned to the carbon-centered radical **IB2**, whose small couplings are not resolved.
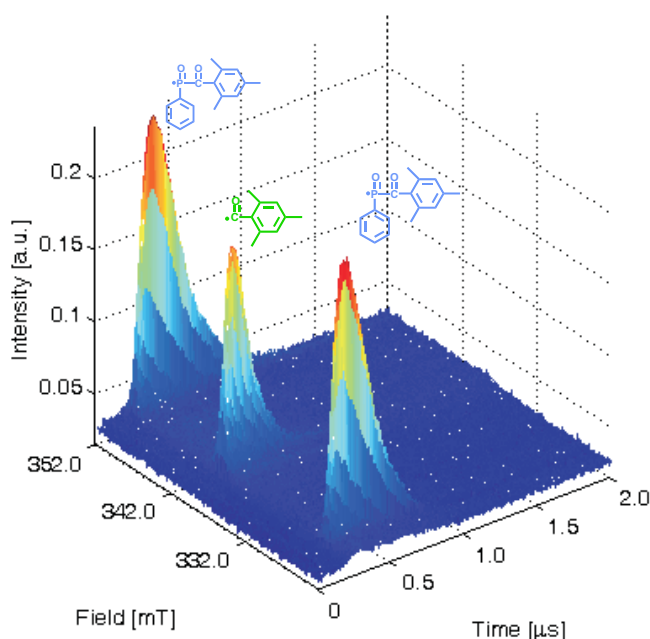
Figure 2.6: TR-EPR spectrum of an argon saturated toluene solution of **I2** at room temperature.

The time-resolved EPR spectrum of photolyzed **I1** in the beginning consists of an absorptively polarized doublet with a typical phosphorous hyperfine coupling constants ($a_p = 36.3$ mT) assigned to **IP1** and an absorptively polarized singlet, assigned to the **IB1** radical. The substituted benzoyl radical has a rather short effective relaxation time (its signal disappears at (t $\geq$ 1 μs), and time-resolved EPR spectrum of **I1** at longer times of observation consists mainly of **IP1** signals. Due to the contribution of S-T$_0$ or RPM to the polarization, the low filed line of **IP1** turns in to emission (Figure 2.7).

18

This manifests the principally known phenomenon of succession of RPM of CIDEP to TM.[27–29]

Figure 2.7: TR-EPR spectra recorded (a) 200-300 ns and (b) 750-1000 ns following 355 nm laser excitation of **I1** in deoxygenated toluene solution at 24°C.

In this chapter, we have focused our study on the reactivity of radicals **IP1** and **IP2** toward four different monomers. The structure of the monomers is presented in Figure 2.8. The phosphorus centered radicals **IP1** and **IP2** were generated by laser flash (355 nm) of photoinitiators **I1** and **I2**.
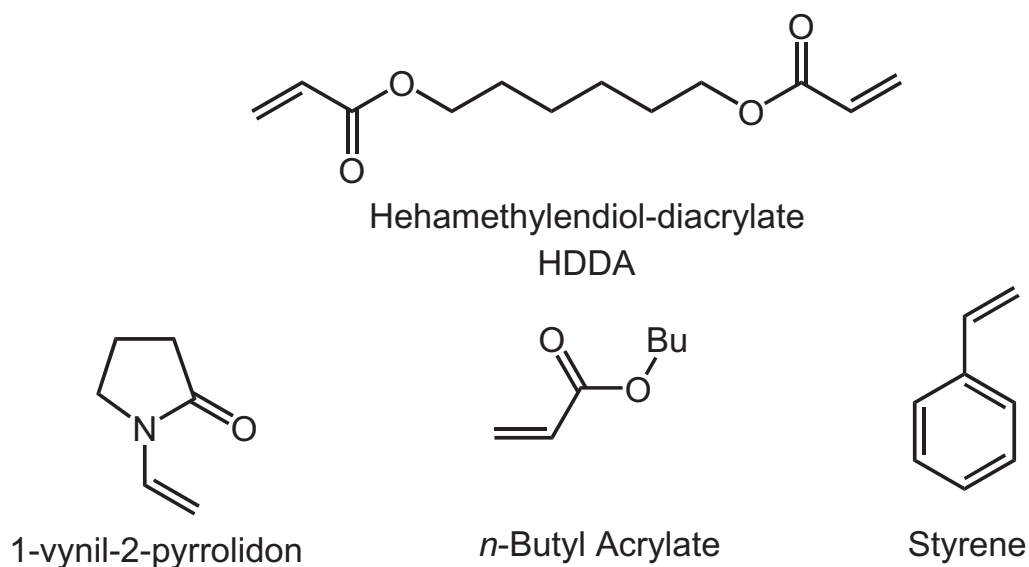
Figure 2.8: Monomers structure.

Both of the radicals (**IP1** and **IB1**) generated after the laser flash of acylphosphine oxide **I1** are able to add to the double bond of the monomer and initiate radical polymerization. Photolysis of an argon-saturated toluene solution of **I1** in the presence of 1-vynil-2-pyrrolidon results in the formation of two different adduct radicals (Figure 2.9).
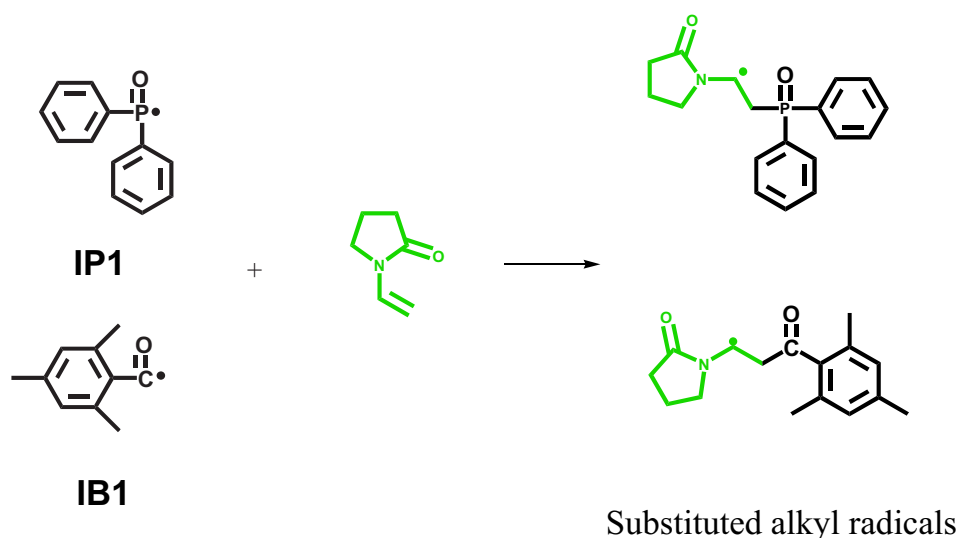
Figure 2.9: Addition of IP1 and IB1 to the double bond of 1-vynil-2-pyrrolidon.

The TR-EPR spectra of argon-saturated toluene solution of **I1** and **I2** 300 ns after laser excitation in the presence of different monomers are shown in Figures 2.10 and 2.11. New signals appeared around the 2,4,6-trimethylbenzoyl radical at about 200 ns after laser flash. These signals are due to the adduct radicals. The new formed adduct radicals are carbon-centered radicals with identical g-values as the benzoyl radical, therefore, their signals appeared around the center field, where the absorption line of the benzoyl radicals is.

The **IB1** and **IB2** radicals have absorptive signals overlapping with the lines of the adduct radicals. It has been found that the benzoyl absorption persists at the same time scale, when signals of **IP1** and **IP2** are almost fully replaced by spin-adduct signals. This observation confirms the conclusion that benzoyl radicals attack the double bond of the monomer at a slower rate than the **IP1** and **IP2** radicals.

Continues-wave EPR measurements of the spin adducts of substituted benzoyl (**IB1** and **IB2**) and phosphinoyl (**IP1** and **IP2**) radicals have shown that the signals of spin adducts of substituted benzoyl radical are weaker than those of phosphinoyl radicals. The reason for that is the lower rates of their formation and the fast rate of relaxation compared to that of phosphinoyl radicals.
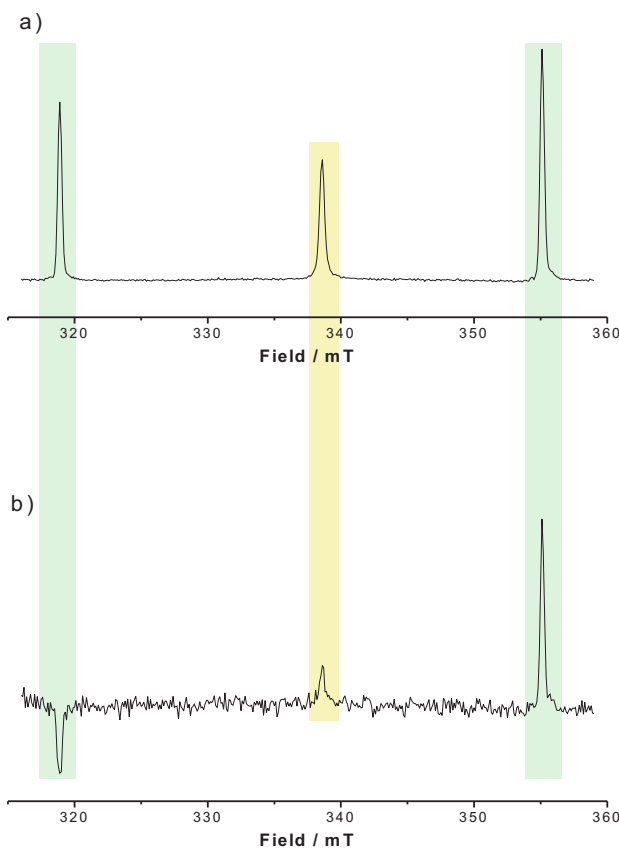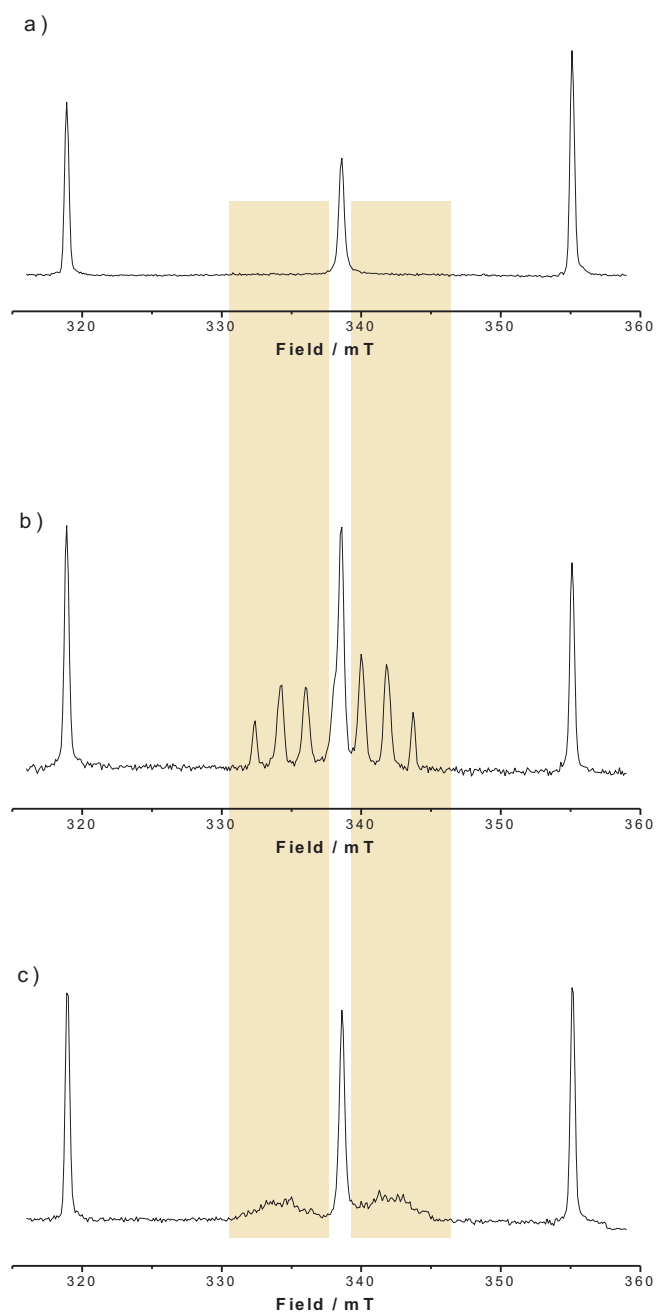
Figure 2.10: TR-EPR spectra recorded 200-300 ns following 355 nm laser excitation of **I1** in deoxygenated toluene solution at 24°C (a) and in the presence of (b) 0.3 M HDDA and (c) 0.4 M 1-vynil-2-pyrrolidon.
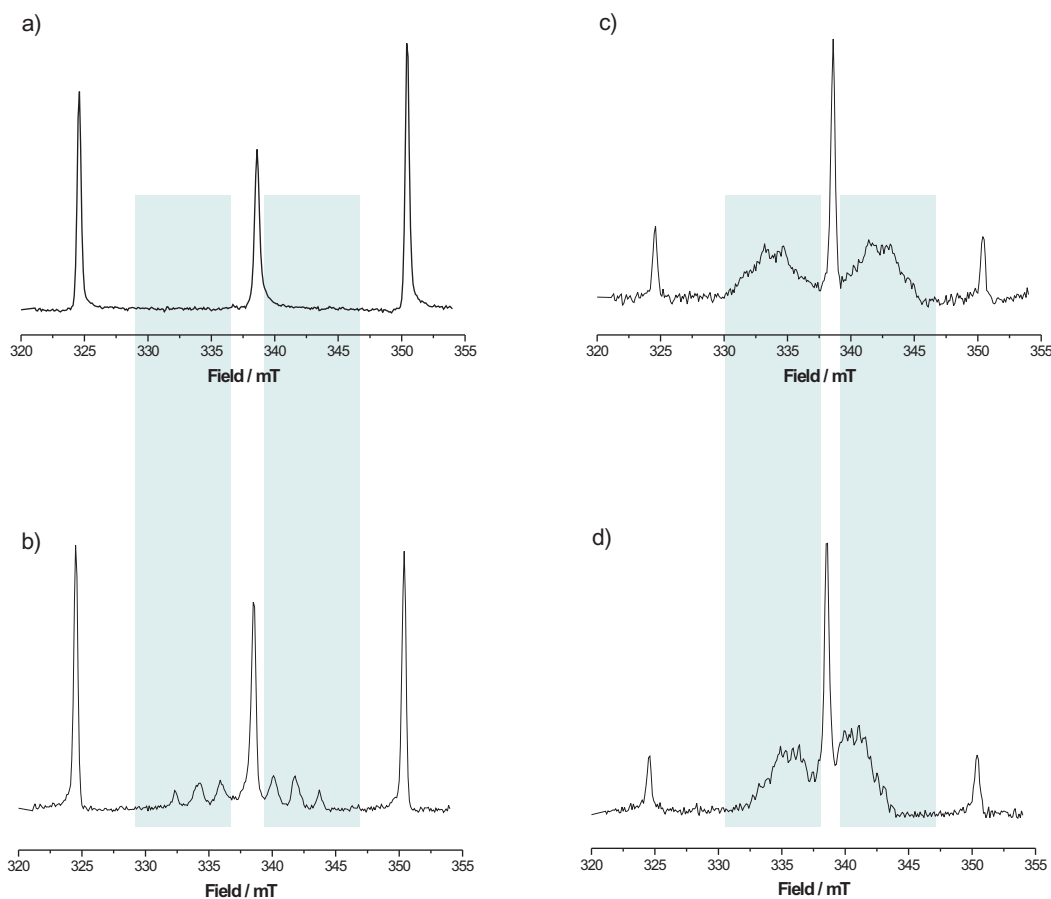
Figure 2.11: TR-EPR spectra recorded 200-300 ns following 355 nm laser excitation of **I2** in deoxygenated toluene solution at 24°C (a) and in the presence of (b) 0.3 M HDDA, (c) 0.4 M 1-vynil-2-pyrrolidon and (d) 0.2 M styrene.

Decays of EPR signals due to the diphenylphosphonyl radical **IP1** in the presence of varing concentrations of 1-vynil-2-pyrrolidon are shown in Figure 2.12. The decays become faster with increasing concentration of the monomer.

As it is mentioned in the chapter-theoretical part, time-resolved continuous-wave EPR detects the radical signal without use of the field modulation of the

spectrometer and has, therefore, a higher time resolution but requires strong spin polarization to ensure suitable signal-to-noise characteristics. The time profile of the signal is influenced by the spin polarization and theoretical analysis require knowledge of the mechanism of electron spin relaxation for the radicals under study. Therefor, the extraction of rate constants from intensity-time profile is tedious and time consuming.[30–33]

Figure 2.12: Time profile of EPR signal intensities due to the diphenylphosphonyl radicals **IP1** in the presence of varying concentrations of 1-vynil-2-pyrrolidon.

A favorable approach is to determine absolute rate constants from TR-EPR spectra by analyzing the line width of the reacting radical in dependence of the quencher concentration. The "line width method" for the determination the addition rate constant of radicals to monomers has been recently introduced by Gescheidt and coworkers.

Line widths of EPR signals of the diphenylphosphinoyl radicals in the presence of varying concentrations of 1-vynil-2-pyrrolidon are shown in Figure 2.13. The line width becomes bigger with increasing concentration of the

24

monomer. This observation can be traced back to a shorter lifetime of the phosphinoyl radical as indicated in the theoretical part.
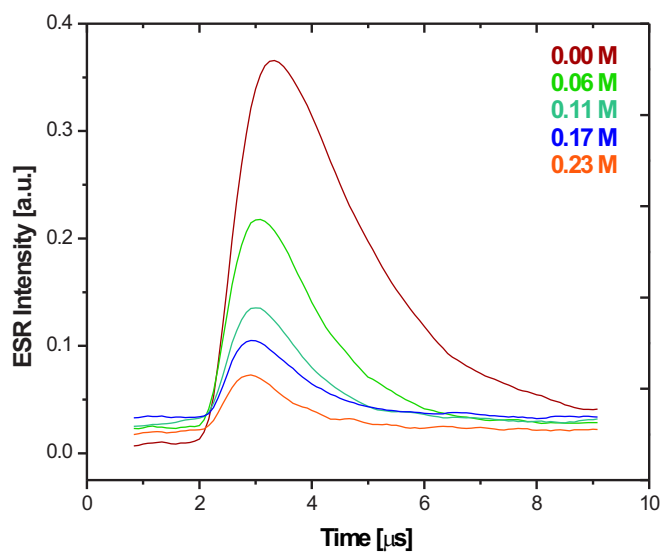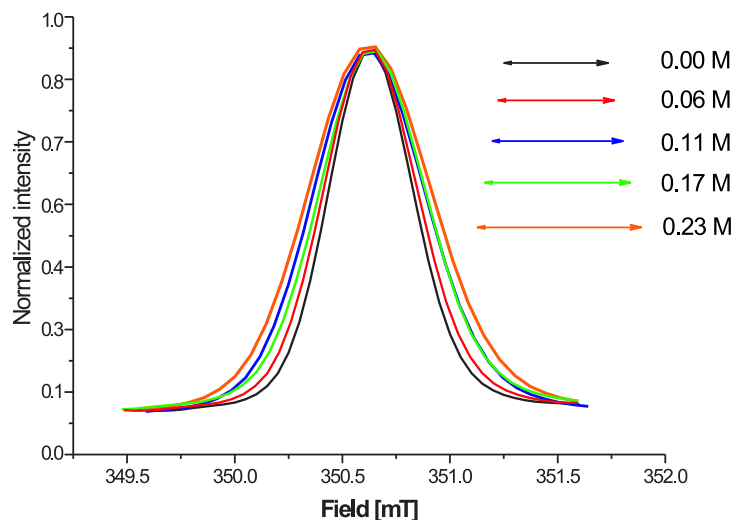

Figure 2.13: Line widths of EPR signal due to the diphenylphosphinoyl radical **IP1** in the presence of varying concentrations of 1-vynil-2-pyrrolidon.

The shape of the lines was analyzed by nonlinear least-squares fitting to *Gaussian* line shape (Equation 2.1). We have chosen it, because the Gaussian line shape lead to a better fit of the experimental data compared with Lorentzian line shape.

$$Y(B) = Y_{max} \cdot \exp[-\ln 2 \cdot \frac{(B - B_0)^2}{\omega^2}] \tag{2.1}$$

where Y(B) is the TR CW EPR signal intensity at the magnetic field position B, Y_{max} is the maximum signal intensity of the EPR resonance line at the magnetic field position B_0, and $\omega = 1/T_2$ is the total line width.

The time dependance of the EPR line width of initiator **I1**, measured after the laser pulse in the absence of a monomer, together with the time profile of the EPR intensity is shown in Figure 2.14. During the first 250 ns, line broadening due to the initial spread of microwave is dominant and after approximately 600 ns, the initially polarized EPR signal has relaxed. Therefore, a time interval between approximately 300 and 500 ns was chosen for the accurate determination of the rate constant.
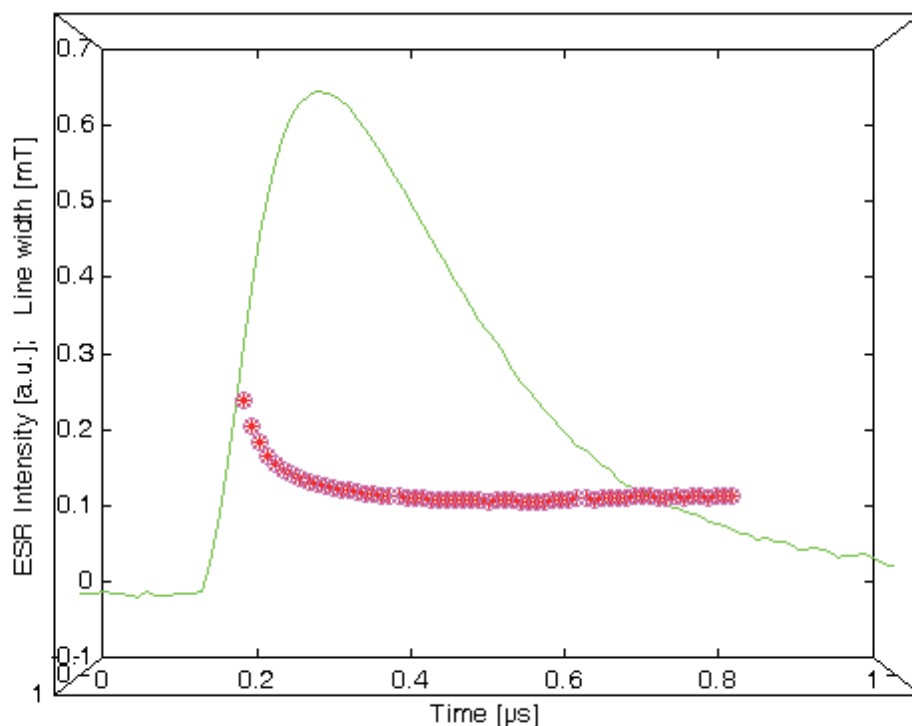
Figure 2.14: High-field resonance line of initiator **I1**: time response of EPR-intensity and line width.

In formulations for technical applications the monomers are present at much higher concentration inside the solution than the initiator molecule (ca. 10^3-fold excess), therefore, the reaction doesn't depend on the monomer

concentration. The kinetic description for this reaction is a pseudo-first-order process. The addition rate constants k_{add} were obtained from plots of the line broadening versus the monomer concentration [M] (Equation 2.2).

$$\frac{1}{T_2} = k_0 + k_{add}[M] \tag{2.2}$$

where k_0 is the monomer independent line width. Figure 2.15 and Figure 2.16 show the resulting linear plots chemical lifetime vs [M] for the addition of **IP1** and **IP2** to 1-vynil-2-pyrrolidon, styrene and hexamethylendiol-diacrylate (HDDA). The rate constants determined from these linear plots are presented in Table 2.2 together with their hyperfine coupling constants.
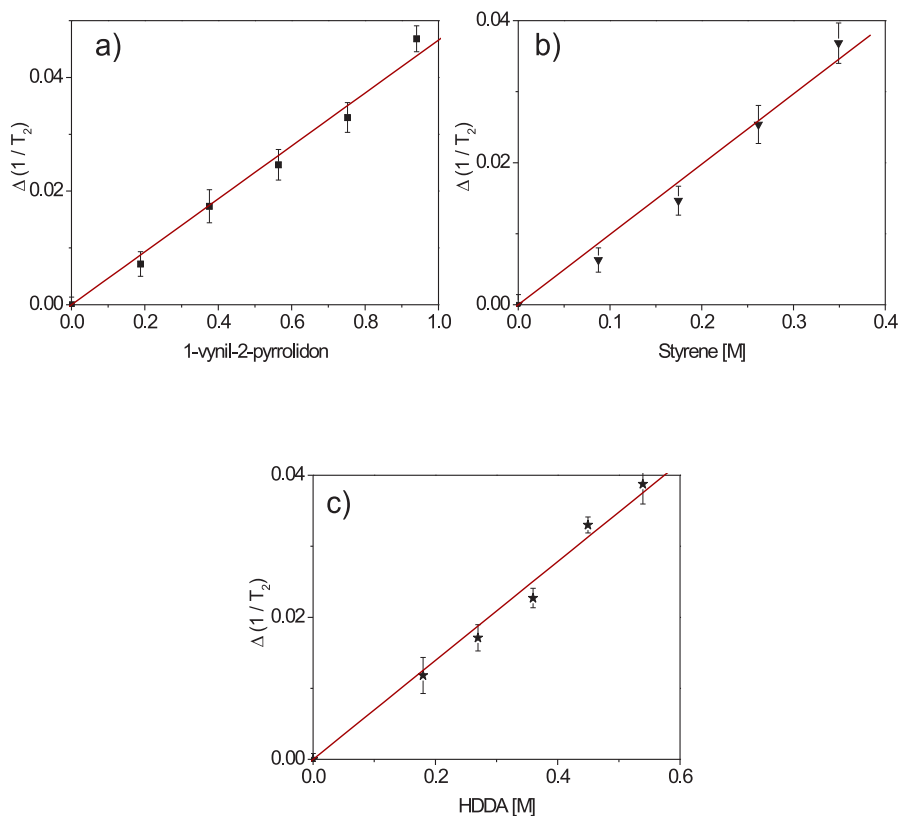
Figure 2.15: Plots of the chemical lifetimes vs. concentration of: (1) 1-vynil-2-pyrrolidon, (b) styrene and (c) HDDA, for the determination of rate constants k_{add} from TR-EPR spectra at X band for radical **IP1**.

Figure 2.16: Plots of the chemical lifetimes vs. concentration of: (1) 1-vynil-2-pyrrolidon, (b) styrene and (c) HDDA, for the determination of rate constants k_{add} from TR-EPR spectra at X band for radical **IP2**.

Table 2.2: ^{31}P hfc's and Addition Rate Constants k_{add} for the Addition of Phosphinoyl Radicals **IP1** and **IP2** to n-Butyl Acrylate, HDDA, Styrene and 1-Vynil-2-pyrrolidon.
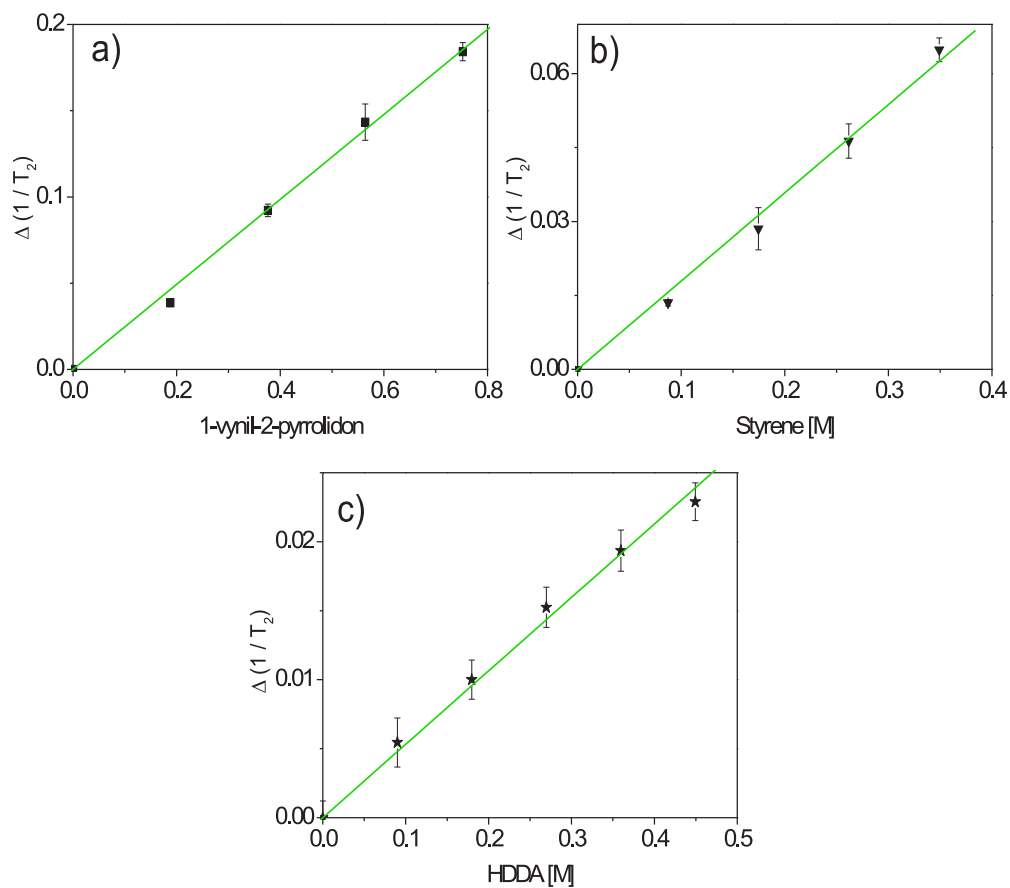
The TR-EPR studies provide key information linking the structure and reactivity of **IP1** and **IP2**. The high reactivity of phosphinoyl radicals has been attributed to their non-planar structure as a result of high degree of s-character and spin localization on the phosphorus atom. The smaller ^{31}P hfc of **IP2** compared to **IP1** indicates the changes to a more planer structure which leads to an increasing p-character of the orbital containing the unpaired electron, and to spin delocalization into the conjugated substituents of the phosphinoyl radical (Figure 2.17). Therefore, a more planar structure results in lower reactivity towards the radical trapping reagents.

IP1   IP2
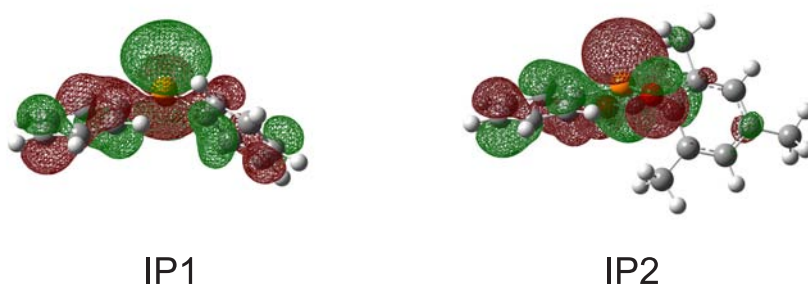
Figure 2.17: HOMO orbitals visualization of **IP1** and **IP2**.

Figure 2.18 shows the comparison between the reaction rate constants of **IP1** and **IP2** towards four different monomers. It can be seen that for the reaction with three of the monomers, the rate constants of **IP1** and **IP2** correlate with the ^{31}P hyperfine coupling. The only exception is in the case of the reaction with 1-vynil-2-pyrrolidon where **IP2** reacts faster than **IP1**. This unexpected result can be rationalized by theoretical calculations. Quantum chemical calculations using B3LYP/6.31G* level of theory show that the propagating radical in the case of styrene is stabilized by higher

delocalization over the substituent (Figure 2.19) compared to the one in the case of n-butyl-acrylat, HDDA and 1-vynil-2-pyrrolidon. This could be the reason for the higher addition rate constants of both radicals to styrene than in the other reactions. Unexpectedly, the addition rate constants of **IP1** towards n-butyl acrylate and HDDA are identical. It is true for the other phosphinoyl radical (**IP2**) too. The reason for it could be the more bulky molecule of HDDA which increase the viscosity at higher monomer concentrations and decrease the mobility of initiator molecule. In the case of n-butyl acrylate, styrene and 1-vynil-2-pyrrolidon viscosity doesn't change at the measured concentrations.

Figure 2.18: Comparison of the addition rate constants of **IP1** and **IP2** to n-butyl acrylate, HDDA, styrene and 1-vynil-2-pyrrolidon.
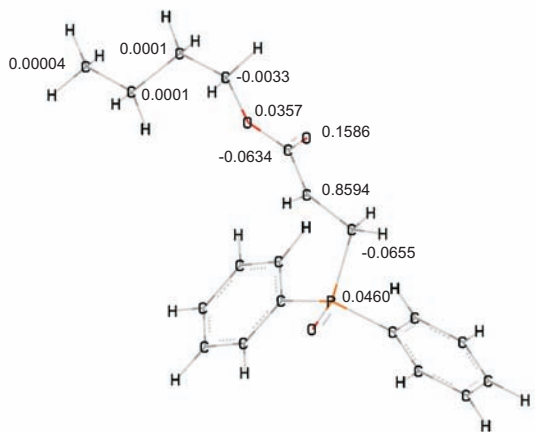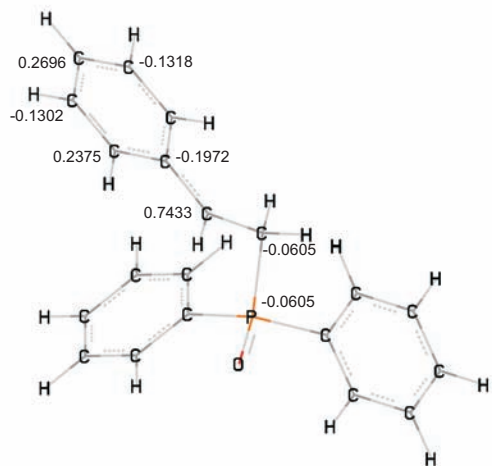
Figure 2.19: Spin density on the two adduct radicals of **IP1** generated after the first addition to the double bond of styrene and n-butyl acrylate.

2.4   Conclusions

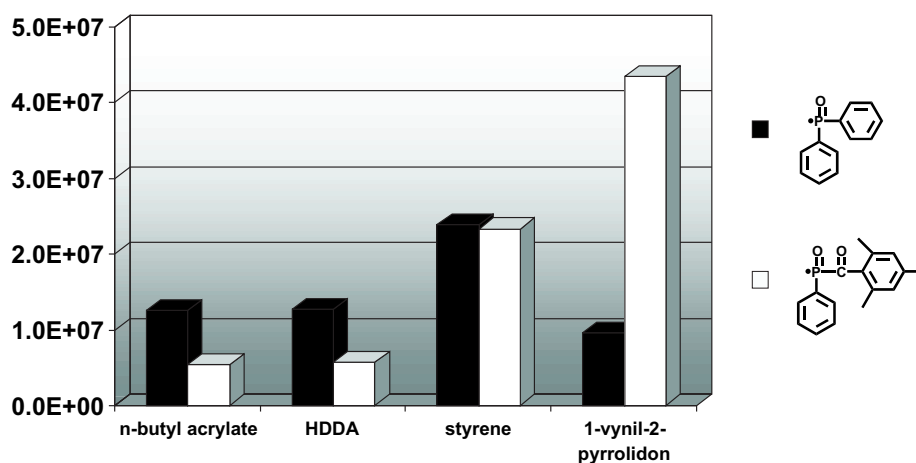The photochemistry of mono- and bis(acyl)phosphine oxides **I1** and **I2** involves α-cleavage from a triplet excited state to afford radicals **IP1**, **IP2** and **IB1** which are readily detectable by TR-EPR.The phosphinoyl radicals **IP1** and **IP2** were characterized by time-resolved EPR in toluene solution and their addition rate constants to n-butyl acrylate, hexamethylendiol-diacrylate, styrene and 1-vynil-2-pyrrolidon were determined by the analysis of the EPR line width. The addition rate constants range from 0.5 x 10^7 to 4.3 x 10^7. This high reactivity is the basis of their efficiency as photoinitiators for free radical polymerization. The difference in the rate constants can be explained with different degrees of spin distribution and s-character at the phosphorus atom. A physical parameter, which reflects this degree of radical localization, is the ^{31}P hyperfine coupling constant. The lower reactivity and smaller ^{31}P hfc of **IP2** compared to **IP1** is consistent with the former having a more planar geometry. The experiments outlined in this chapter have demonstrated the power of TR-EPR to probe photopolymerization initiation. This method allows the determination of the addition rate constants of the radicals to the double bond of the monomer and also provides structural information of the reactive species. DFT calculations, which may give the possibility to rationalize the relative rates of these reactions are in progress. We finish this work with an open question: Why **IP2** reacts faster with 1-vynil-2-pyrrolidon than **IP1**?

Chapter 3

Benzoyl radicals

3.1 Benzoyl radicals

3.1.1 Introduction

The class of initiators involving free radicals represents more than 90% of the commercially used initiators. Free radical initiators are most typically used with acrylate/methacrylate functional resins and can also be used with unsaturated polyester resins.

With the growth of this technology in manifold applications, a large variety of photoinitiators has been developed. Acylphosphine oxides and α-amino ketones are two different classes of photoinitiators that have found wide application in industry. Upon absorption of a photon of suitable wavelength, these photoinitiators undergo homolytic bond cleavage from a triplet excited state to produce two different reactive radicals. [34] This is illustrated in Figure 3.1 for a monoacylphosphine oxide and α-amino ketone.

The addition of these radicals to alkenes and other unsaturated compounds leads to the creation of new carbon-carbon σ bonds at the expense of existing π bonds. [35–38] The reaction rates and selectivities vary considerably, and depend on the substitution of both the substrate and the radical. Such rate variations may result in the success or failure of the product, and therefore a predictive synthetic strategy can be developed when the rate constants for the addition, and the factors controlling them are known.

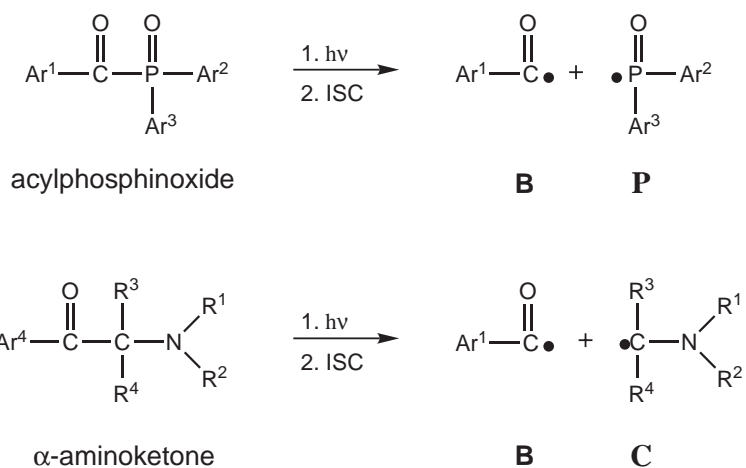The addition of these primary radicals to n-butyl acrylate is shown on Figure 3.2.

Figure 3.1: Formation of the primary radicals from acylphosphinoxide and α-aminoketone-type photoinitiators
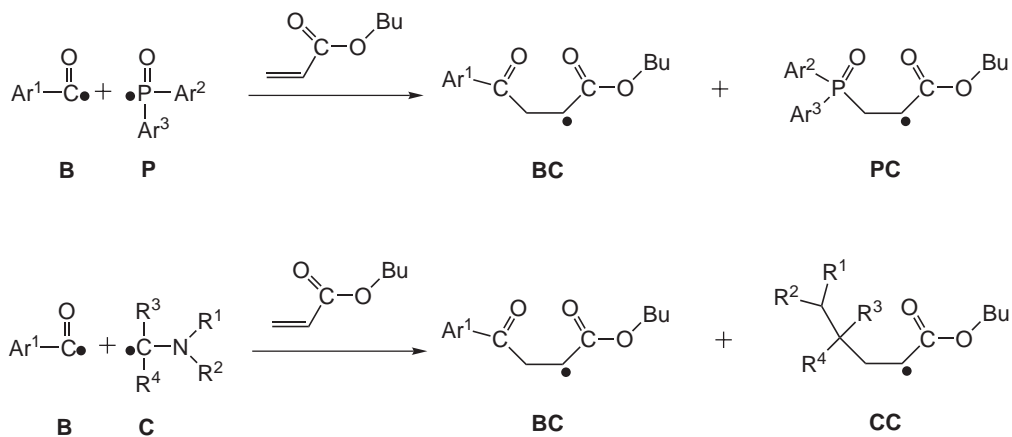

Figure 3.2: First addition of the radicals to the double bond of n-butylacrylate

This first reaction step is important for the efficiency of a photoinitiator and, therefore, the accurate experimental determinations of absolute rate constants for radical reactions, their activation parameters, quantum-chemical calculations of transition state structures and reaction barriers are of particular interest.

There are already existing data for several phosphorus centered and α-amino C-centered radicals, but the information about the most frequently occurring benzoyl radicals is only scarce. The reason for this lack of information is that the optical absorption of these species is hardly detectable by UV-VIS spectroscopy. Unfortunately, benzoyl radicals have a low extinction coefficient at wavelengths higher than 300 nm and therefore is very difficult to detect them directly by laser flash photolysis employing optical methods. In addition, overlapping optical absorptions of the initiator molecule and the benzoyl radical complicate the kinetic analysis with optical detection methods. It has been demonstrated that time-resolved infrared spectroscopy can be used for the direct detection of benzoyl and aliphatic acyl radicals due to the fact that these radicals have well-resolved vibrational absorptions.

The electron paramagnetic resonance (EPR) technique provides a powerful tool for investigating the reactivity of radicals because it not only allows direct observation of the radicals but also gives structural and dynamic information on these species. We have used time-resolved continuous-wave EPR as a tool for determination the addition rate constant of five different benzoyl radicals to the double bond of n-butyl acrylate.

3.1.2   Compounds Investigated

For UV-curing of pigmented systems, photoinitiators having absorption at longer wavelength are required. α-Aminoketones are such a class of photoinitiator that have found application for UV-curing of pigmented systems, since they absorb light of wavelengths at which the formulation is transparent.

Acylphosphine oxides are another class of photoinitiators highly suited for white lacquers, as their absorption spectra extend well into the visible light region and they do not produce yellowing.

In the following chapter we have investigated the addition rate constant of five different benzoyl radicals derived from two bisacylphosphine oxide

photoinitiators and three α-amino ketones phtoinitiators. The structure of these compounds is shown in Figure 3.1.5.
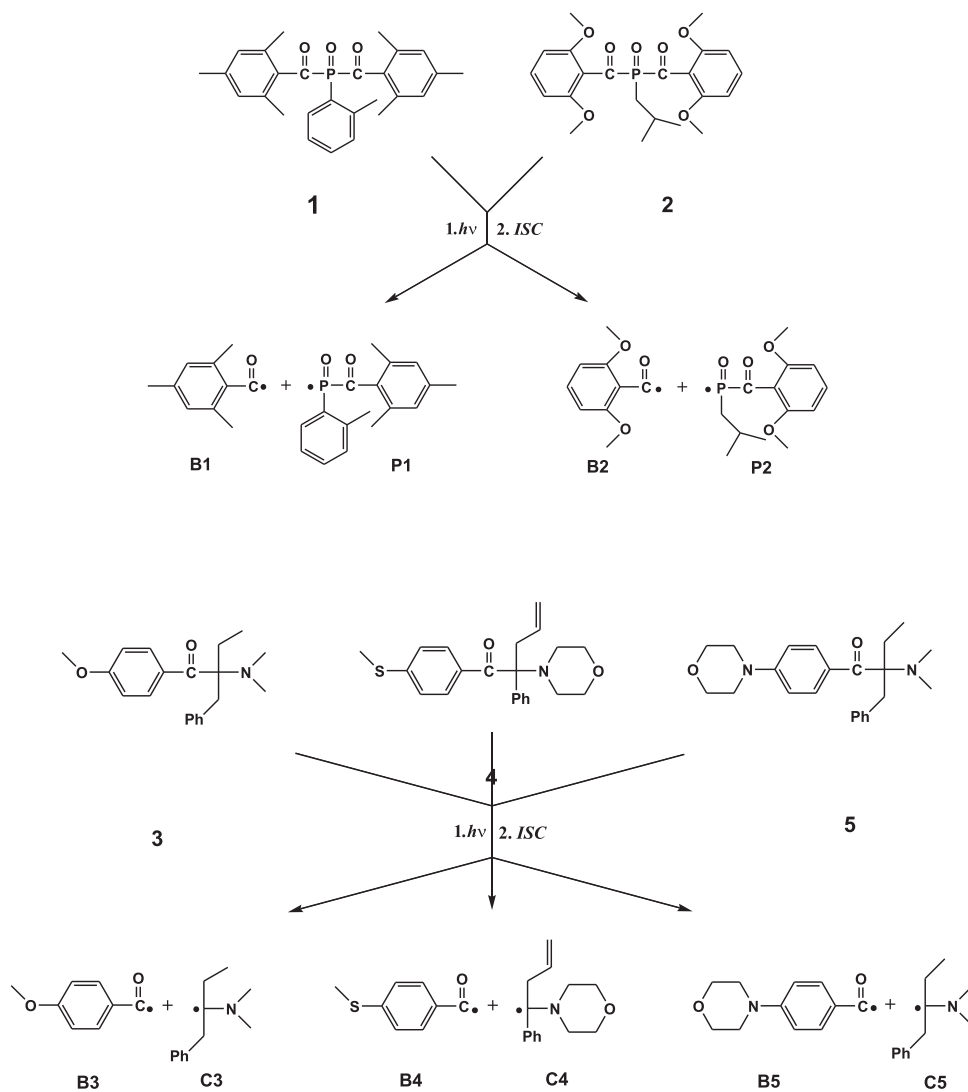
Figure 3.3: α-cleavage of the studied photoinitiators

36

3.1.3 Absorption Spectra

The effective absorption of UV light by the photoinitiator is one major condition for the efficient cure of UV systems. The alpha-cleavage initiators are typically differentiated by their absorption profiles. Figure 3.4 shows the UV absorption spectra of the three studied α-amino ketone photoinitiators.
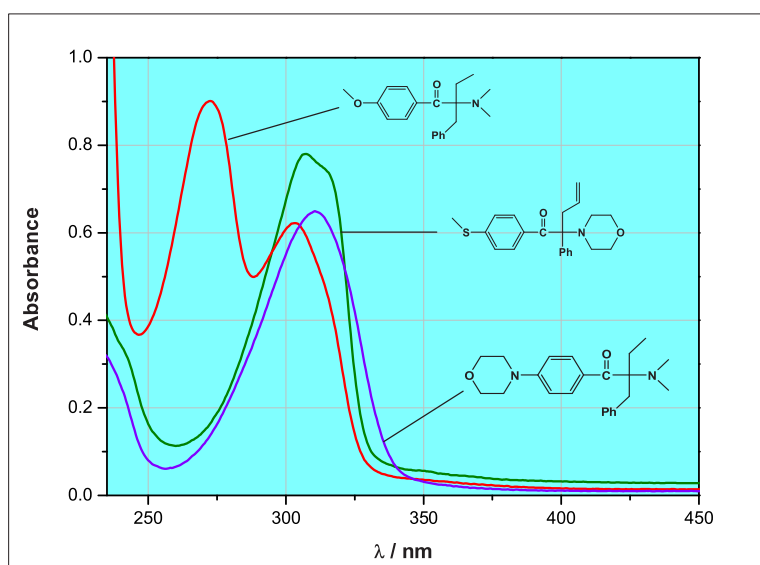
Figure 3.4: UV absorption spectra of three different α-amino ketones in n-hexane.

Introduction of electron donating substituents such as methoxy, methylthio or amino groups in the para position induces a red-shift of the main absorption band towards longer wavelength compared to the spectra of photoinitiators possessing a non-substituted benzoyl moiety. The thio or amino substituents induce strong charge transfer characteristics to the excited state and the absorption maxima are situated around 307 and 322 nm, respectively. Compared to thiomethyl substituent, the maximum of the main absorption band is still further red-shifted by the p-morpholino group.

The absorption spectra of α-amino ketone photoinitiators is influenced not only by the substituents on p-position of the benzoyl moiety, but also by the substituents at the α-position. The difference is that these substituents do

not change the position of the main absorption band, but lead to an expansion of this band into the visible region. This allows application of light above 350 nm.

The absorption characteristics of bisacylphosphine oxides photoinitiators differ from the one of α-amino ketone type. They show enhanced absorption in the near UV/visible range. Spectrum of a photoinitiator of this type is shown in Figure3.5.
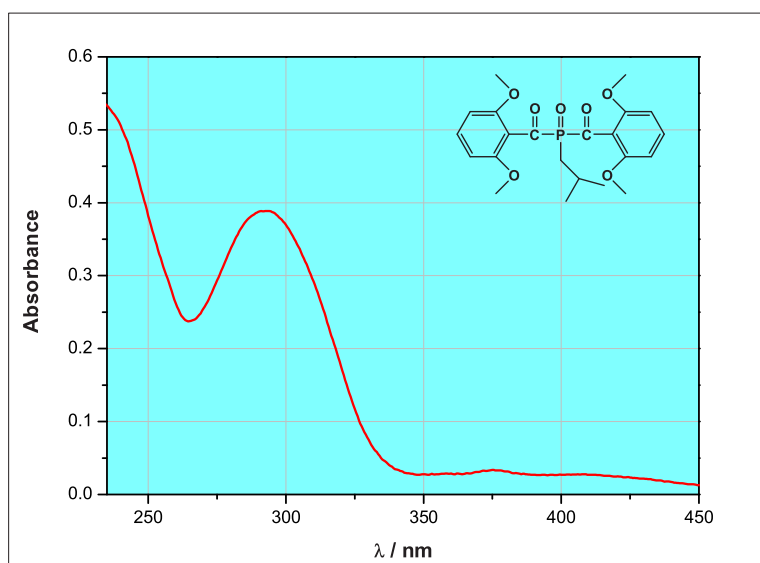
Figure 3.5: UV absorption spectra of BAPO in n-hexane.

3.1.4   Previous Studies

Bis(acyl)phosphine oxides upon irradiation undergo α-cleavage with high efficiency ($\Phi_\alpha \approx 0.6$) to produce a benzoyl-phosphinoyl radical pair. They are highly effective photoinitiators since they can (in principle) produce four radicals, each of which is an efficient initiator.

Laser flash photolysis (355 nm excitation) of the phosphorus photoinitiator **2** affords readily detectable transient absorption spectra, by TR-EPR, which decay on the microsecond time scale with mixed kinetics and have been

assigned to the phosphinoyl radical. (Acyl)phosphinoyl radicals show strong transient absorptions at about 450 nm and another one at 330 nm, which is caused by the phenyl substituents on the phosphorus. The benzoyl radicals **B1** and **B2** do not interfere with the kinetics since they possess only a very weak absorption in the area where the phosphorus radicals absorb.

The high reactivity of phosphinoyl radicals towards unsaturated compounds has been a subject of lots of studies during the past years. Several model reactions of hydrogen abstraction and electron-transfer have been also studied and the data are already published in the literature. The addition rate constants for these reactions are summerised in Table 3.1.[38–41]
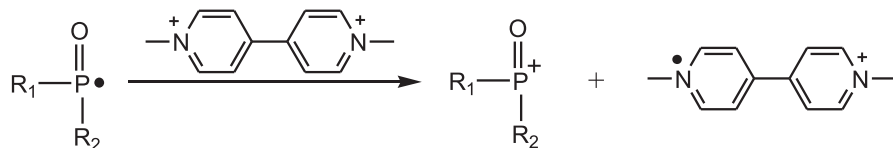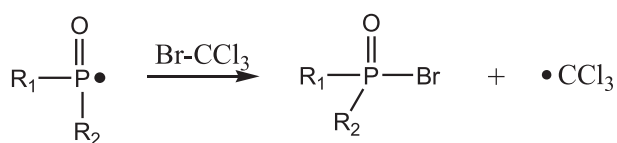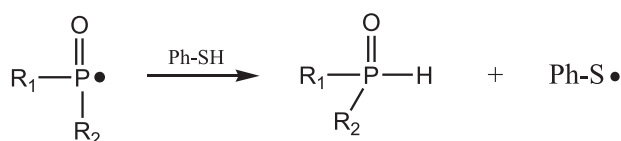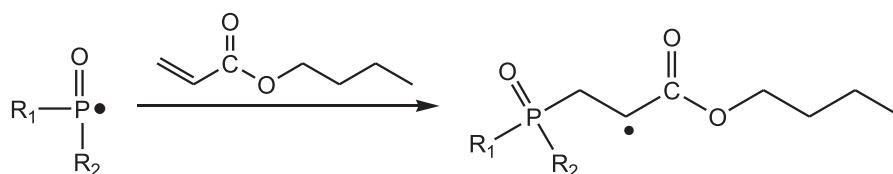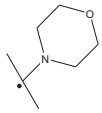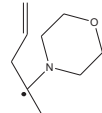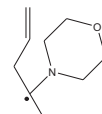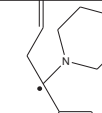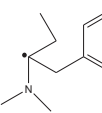
Table 3.1: Rate Constants for Reaction of 2,4,6-Trimethylbenzoyl Radical with Bromotrichloromethane (BrCCl$_3$), Thiophenol (PhSH) and Benzhydrol (Ph$_2$CHOH) in Alkane Solution at 23 ± 2°C.

Reagent	k_q (10^{-8} Ms)
BrCCl$_3$	1.7
PhSH	0.13
Ph$_2$CHOH	<0.005

α-amino ketones undergo α-cleavage to produce benzoyl and α-amino radicals. Consequently, the factors controlling there reactivity towards alkenes have been the subject of much experimental and theoretical work. Unfortunately, these radicals have low extinction coefficients at wavelength higher than 300 nm, and are therefore difficult to detect directly by laser flash photolysis. Recently it has been shown that the difficulty with the low extinction coefficient of the benzoyl radicals can be easily overcome using time-resolved infrared (TRIR) spectroscopy.[41–43]

To overcome this problem in the case of the ketyl α-amino radicals, Turro and coworkers developed an indirect optical method for determination of their addition rate constants to an acrylate monomer. This method is based on the use of a probe, which can react selectively and rapidly with these radicals, leading to easyly detectable intermediates by optical absorption spectroscopy. As such a probe they have used crystal violet. The data which they have obtained for the reactivity of several α-amino radicals towards n-butyl acrylate and oxygen is summarized in Table 3.2.

Table 3.2: Rate Constants for Addition of α-Amino Radicals to n-Butylacrylate and Oxygen in Acetonitrile Solution at 23 and 24° C.

	$K_{acrylate}$ $(10^6 \text{ M}^{-1} \text{ s}^{-1})$	K_{oxygen} $(10^9 \text{ M}^{-1} \text{ s}^{-1})$
	29	6.3
	18	4.5
	7.5	3.9
	< 0.1	2.3
	6.1	4.3

3.1.5 TR-EPR Studies

The academic and industrial interest in α-amino ketones and acylphosphin oxide photoinitiators comes from the high reactivity of the formed radicals after laser flash toward alkenes. Consequently, factors controlling the rate constants have been the subject of much experimental and theoretical work.

The addition rate constants of five different carbon-centered radicals to the double bond of n-butyl acrylate were studied by TR-EPR technique. It has

been shown in the previous chapter, that the rate constants of the radicals can readily be determined by line-width measurements in continuous-wave time-resolved EPR spectra at X-band. This method has been established for determination the addition rate constants of phosphorus-centered radicals.

Benzoyl radicals are the most frequently appearing radicals and there time-resolved-EPR spectra can easily be detected. However, it still remains a challenge to establish their reactivity. Although their EPR signals are readily detectable, their kinetic analysis is not easy. The reason for it is that the reactivity of benzoyl radicals toward alkenes, which is an important step in free radical polymerization, is much slower than, *e.g.*, the phosphinoyl radicals. This leads to smaller variations in the line-width ($1/T_2^*$ - $1/T_2^0$) of the CW-TR-EPR spectra depending on the quencher concentration. In addition to it, the small changes in the line-width cause bigger error margins. This can be overcome by increasing the number of measurements and the data points for the analysis.

To investigate the reactivity of these radicals in more details, W-band EPR measurements were performed and compared with the results from the one at X-band EPR. W-band EPR gives the possibility to observe the radicals in thermal equilibrium. The analysis of the time dependence of the EPR time profile may yield directly the kinetic information about the radical reactions. Consequently, two EPR approaches are envisaged to determine the chemical lifetime from Equation .The first one is to measure the line broadening ($1/T_2^*$ - $1/T_2^0$) by X-band EPR when varying the monomer concentration [M] and the second one to measure time profile of W-band EPR intensities depending on this concentration [M].[42, 44–46]

An additional complication which occurs is that the second radical from the primarily formed radical pair after the laser flash has a considerably higher reactivity than the benzoyl radical and predominantly consumes the alkene monomer. This may result in changing the first-order rate low of the addition reaction of benzoyl radical to n-butyl acrylate.

To avoid this complication, we have chosen five different photoinitiator molecules in the way, that the second radical from the radical pair, formed after the laser flash has as smaller reactivity as possible. The compounds shown on Figure fulfil this requirement. The photolysis of the five initiator molecules yields five different benzoyl radicals with an 2,4,6-trimethylphenyl (**B1**), 2,6-dimethoxyphenyl (**B2**), 4-methoxyphenyl (**B3**), 4-thiomethylphenyl (**B4**)

and 4-morpholinophenyl (**B5**) substituents. The first two compounds shown on this figure are bisacylphosphin oxides. The phosphorus centered radicals **P1** and **P2**, generated after the laser flash are sterically hindered by aryl or branched alkyl groups which slow down there reactivity. This was shown in previous investigations and there addition constants to n-butyl acrylate are $8 \cdot 10^5$ M$^{-1} \cdot$s^{-1} and $1.8 \cdot 10^6$ M$^{-1} \cdot$s^{-1}. The same is true for the α-amino C-centered radicals, formed from the three α-amino ketone photoinitiators, **C3**,**C4** and **C5** which have the addition rate constant $6.1 \cdot 10^6$ M$^{-1} \cdot$s^{-1}, $1 \cdot 10^5$ M$^{-1} \cdot$s^{-1} and $6.1 \cdot 10^6$ M$^{-1} \cdot$s^{-1} respectively.

Laser flash photolysis of toluene solution of photoinitiator **1** affords the TR-EPR spectrum shown in Figure 3.6. The spectrum features a doublet due to the phosphinoyl radical **P1**, these are the two lines at the edge of the spectra, and a broad absorption line near center field assigned to benzoyl radical **B1**. The EPR signals of both radical species are well separated due to the dominating isotropic hyperfine coupling constant (hfc) of the ^{31}P nucleus.
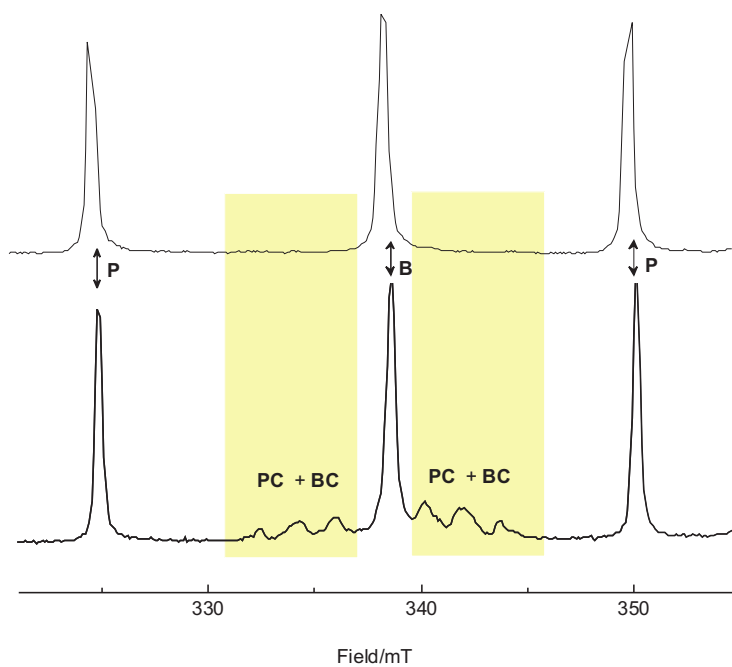
Figure 3.6: X-band TR-EPR spectra of **1** (0.01 M) in toluene a) without and b) with butyl acrylate (2.8 M) observed 200-300 ns after laser flash.

The TR-EPR spectrum recorded 200-300 ns after 355 nm laser excitation of photoinitiator **1** in toluene solution containing 2.8 M concentration n-butyl acrylate is shown on Figure 3.6 together with the TR-EPR signal of the same photoinitiator without the presence of the monomer. The main feature of the spectrum is the complex absorptive multiplet near center field assigned to the benzoyl radicals **PC** and **BC**, formed after the first addition of the initiator radicals to the double bond of n-butyl acrylate. An absorptive doublet due to unreacted **P1** radical and the singlet due to unreacted **B1** radical are also presented. The X-band EPR signals from the new formed radicals **PC**,**CC** and **BC** partially overlap with those of the benzoyl radicals **B**, but its line-width is not substantially affected by the overlap of EPR lines Figure 3.6 and 3.7 a).

Figure 3.7 shows X- and W- band TR-EPR spectra recorded after laser flash photolysis at 355nm of photoinitiator **5** in the absence of n-butyl acrylate. It can be seen that there is an overlap of the carbon-centered radicals **C5** and **B5**. The same is true for photoinitiator **3** and **4** . Nevertheless, the signal due to the benzoyl radicals **B** is well distinguishable and their kinetic investigation by means of the TR-EPR line-width method can be performed.
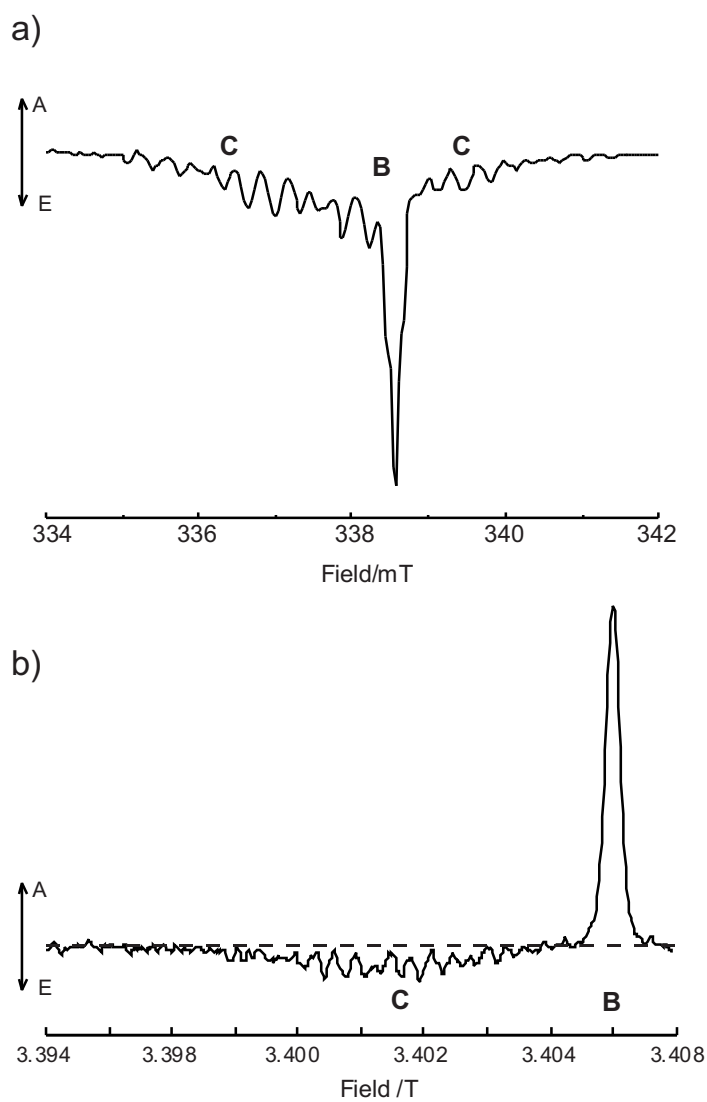
Figure 3.7: TR-EPR spectra recorded after laser flash photolysis of **5** in toluene in the absence of butyl acrylate: a) X-band spectrum: 90 mM concentration of **5** taken 900 ns following laser flash, b) W-band spectrum: 9 mM concentration of **5** taken 200 ns following laser flash.

45

Kinetic Analysis for the Benzoyl Radicals by X-band TR-EPR.
When n-butyl acrylate monomer is present in the toluene solution of the photoinitiator molecule, the EPR line of the benzoyl radical gets broader. Such a line broadening can be easily followed by TR-EPR when changing the concentration of n-butyl acrylate. The TR-EPR signals of the benzoyl radicals, obtained after photolysis of **1** at two different concentrations of butyl acrylate, are shown together with there simulations in Figure 3.8.
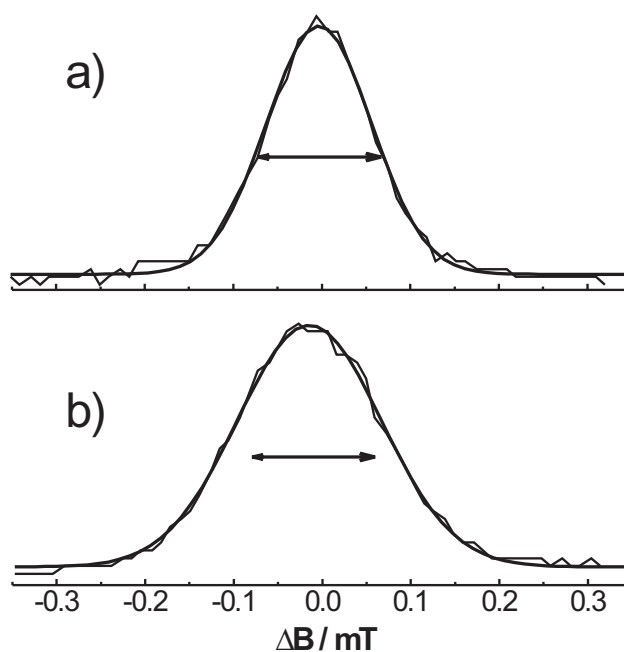
Figure 3.8: X-band TR-EPR spectra of the benzoyl radical **B5** recorded 600 ns after the laser flash. a) 0 M concentration of n-butyl acrylate, b) 2.8 M concentration of n-butyl acrylate. The solid lines show their simulation by Gaussian function with the half width, $\Delta B_{1/2} = 0.0842$ (a) and 0.0947 (b) mT. The arrows in a) and b) posses identical lengths and indicate the amount of the line broadening.

The reactivity of the benzoyl radicals **B1-B5** were determined by analysis of the line broadening of their EPR signals. In the presence of radical quenchers, such as n-butyl acrylate, the lifetime of the benzoyl radicals decreases due to the addition to the olefin. At relatively high n-butyl acrylate concentrations, the reaction follows pseudo-first-order kinetics. As it was shown in the previous chapter, first-order kinetics translates into a linear relationship between line broadening and monomer concentration.

Analysis of the TR-EPR spectra according to this relation yields the plot chemical lifetime vs. concentration displayed in Figure 3.9.
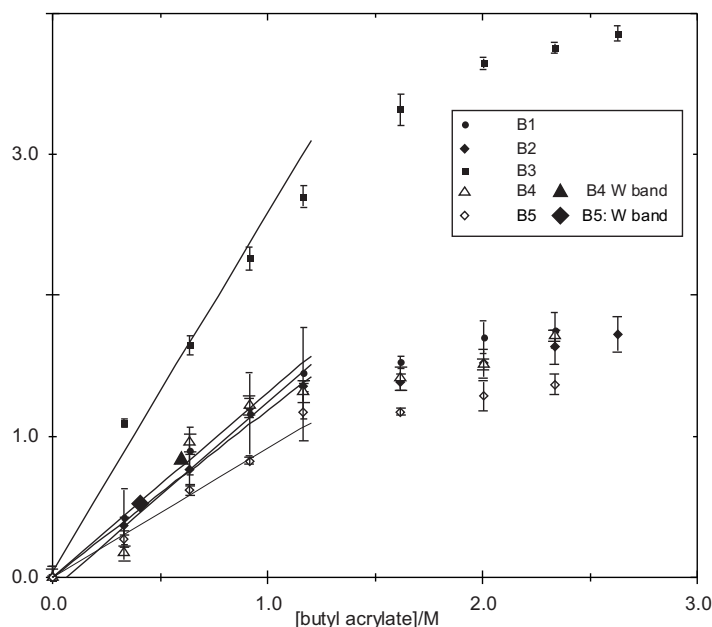
Figure 3.9: Plots of the chemical lifetime *vs.* concentration for the determination of rate constants k_{add} from TR-EPR spectra at X and W band for benzoyl radicals **B1-B5**. The linear relationships are indicated for butyl acrylate concentrations ¡ 1.25 M.

It could be seen from this figure that there is no simple linear relation between the line-width broadening of the EPR signals for benzoyl radicals **B1-B5** and the concentration of the monomer. The whole range between 0 M and 2.8 M concentration of n-butyl acrylate can be separated into two parts. Linear regression for butyl acrylate concentrations below 1.25 M provides,

from the slopes, addition rate constants, k_{add}, of around 10^6 $mol^{-1}s^{-1}$ (Table 3.1.5). At concentrations higher than 1.25 M, the curves lever off and the k_{add} values decrease drastically by up to an order of magnitude.

Table 3.3: g Factors and addition-rate constants, k_{add}, of benzoyl radicals **B1**-**B5** to butyl acrylate, determined by TR-EPR at 9 and 95 GHz. The measurements have been performed in argon saturated toluene solution at room temperature. The absolute error in g-factor measurements is $\pm 5 \cdot 10^{-5}$.

benzoyl radical	g-factor	$k_{add}/ \cdot 10^6$ $mol^{-1}s^{-1}$	$k_{add}/ \cdot 10^5$ $mol^{-1}s^{-1}$
		0.0–1.25 M	1.26–2.7 M
		butyl-acrylate conc.	butyl-acrylate conc.
B1	2.00055	1.18 ± 0.07	4.3 ± 0.7
B2	2.00057	1.25 ± 0.05	4.6 ± 0.7
B3	2.0009	1.91 ± 0.01	3.6 ± 0.5
B4	2.00077	1.25 ± 0.05	5.7 ± 0.8
B5	2.00086	1.03 ± 0.07	7.1 ± 0.2

Addition constants in the range of 10^5-10^6 $mol^{-1}s^{-1}$ are at the limit to be measured by the EPR line-width method because the additional broadening of the EPR lines becomes too small to be detectable by X-band TR-EPR. Moreover, the partial overlap with the spectra of the partner radicals C and the products CC (Figure 3.6 and 3.7) leads to errors in the line-shape analysis. To obtain reference data and to verify the kinetic constants acquired from the X-band TR-EPR spectra , we have additionally performed TR-EPR experiments at high microwave frequency (W-band).

W-Band EPR. Shape of the TR-EPR spectra. In the W-band EPR spectra, the signals belonging to different radicals with different g-factors

show a better separation than at X-band due to the increased Zeeman interaction at 10 times higher magnetic fields. This increased resolution is apparent in Figure 3.7b where the signal of the 4-morpholinobenzoyl radical **B5** is well separated from that of the 1-phenyl-2-(dimethylamino)but-2-yl radical **C5**. Moreover, the W-band spectrum, taken 200 ns after the laser pulse, demonstrates strongly increased spin relaxation at high magnetic field owing to field-dependent fluctuating Zeeman and spin-rotation interactions. Because of fast relaxation, the signal of the benzoyl radical **B5** exhibits practically no transient spin polarization whereas that of the carbon centered radical **C5** is still polarized by the radical pair mechanism.[46–49]

W-band EPR. Kinetic Analysis for the Benzoyl Radical. As was demonstrated earlier the line intensities in the W-band spectra of the benzoyl radicals are virtually free from polarization phenomena and represent the observed radicals at thermal equilibrium. Thus, the chemical-decay rate of the benzoyl radical can be directly determined by recording the time profile of the EPR signal intensity. This is accomplished by subtracting the decay curves, evaluated for the pure photoinitiator (with no butyl acrylate present), from those obtained in the presence of butyl acrylate (Figure 3.9). Because of the high polarity of the reaction solutions at high butyl-acrylate concentrations, the W-band experiments could only be run at low concentrations of the alkene when the solutions were not too lossy for the microwaves. The chemical lifetimes of the radicals at selected concentrations of butyl acrylate measured by the decay of the high-field line intensities are displayed in Figure 3.9 together with the results of the X-band measurements. They are in excellent agreement, thus approving the analysis of the X-band EPR spectra, which could be recorded over the complete range of butyl acrylate concentrations.[50–52]

3.1.6 Reactivity Considerations

We have shown in our study that there are two regions for the reactivity/concentration domain, but what are the reasons causing these two regions? One of the reasons responsible for it could be, that the reaction of these benzoyl radicals with n-butyl acrylate obey second-order rate low. If this is true, than the rate of the reaction is directly proportional to the square of the concentration of one of the reactants. This means, that if we change the concentration of the initiating radicals inside the toluene solution, the line-width should change too. Remarkably, variation of the initiating-radical concentration, either by photolysing differently concentrated photoinitiator solutions, or by varying the laser-light intensity, did not lead to any changes

of the X-band EPR line-widths or W-band EPR decay-profiles. Thus, a second-order rate law is not conceivable.

The second reason for it could be that the physical properties of the reaction mixture vary with changing the butyl acrylate concentration and this leads to a reduced reactivity of the benzoyl radicals. To see if this is the case, we have measured, over the whole concentration range, the viscosity of the toluene solutions used for the TR-EPR measurements. The change of the relative kinematic viscosity and the line-width of the EPR signals versus the butyl acrylate concentration are shown on Figure 3.10.
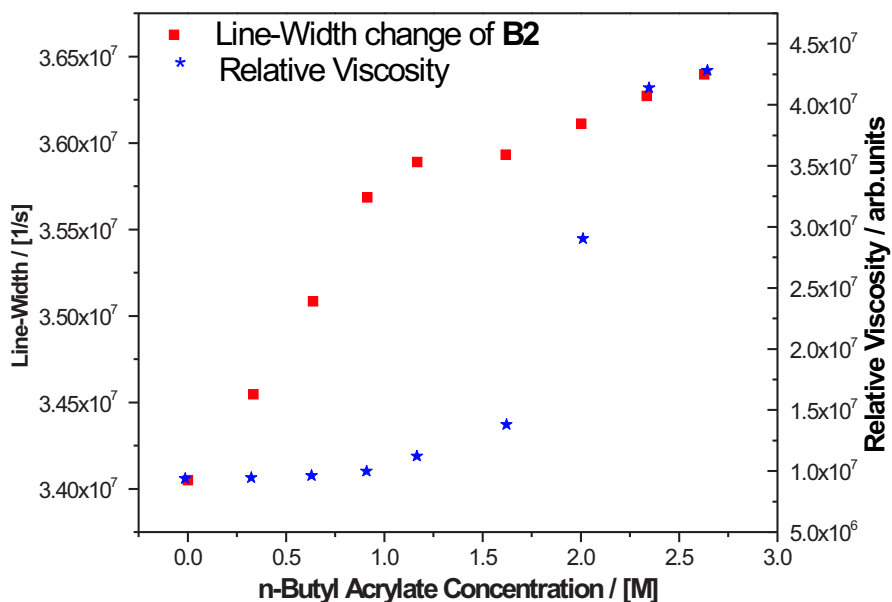
Figure 3.10: Comparison between the dependencies of the rate constants and the relative kinematic viscosity *vs.* n-butyl acrylate concentration of **B2**.

It is clearly visible from the plot in Figure 3.10, that the relative kinematic viscosity drastically increases at n-butyl acrylate concentrations higher than 1.25 M. These are exactly the concentrations at which the reactivity of the benzoyl radical **B2** towards n-butyl acrylate is reduced by approximately one order of magnitude.

Therefore, the reactivity of benzoyl radicals can be divided into two domains. At butyl acrylate concentrations below 1.25 M, the first-order rate constants are ca. one order of magnitude larger than at quencher concentrations above 1.25 M (Table 3.1.5). The values determined for radicals **B1**, **B2**, **B4**, and **B5** in the high-viscosity range by EPR correspond very well with the values determined by time-resolved IR spectroscopy at high concentrations of butyl acrylate.

In the case of the phosphinoyl and the α-amino C-centered radicals, measurements at high monomer concentrations cannot be performed. The reason for it is that both of this type radicals have higher reactivity towards n-butyl acrylate and the decay of the corresponding EPR signals is too fast to be observed in the time window of our experiment. Therefore, comparison of their behavior and the behavior of benzoyl radicals cannot be done.

3.1.7 Correlation Between the Experimental Data and Quantum Chemical Calculations

The data collected in Table 3.1.5 shows that the reactivity of the five benzoyl radicals towards n-butyl acrylate for the low viscosity domain depends on the substituents of the phenyl moiety. It is highest for the 4-methoxybenzoyl radical (**B3**) and lowest for the 4-morpholinobenzoyl (**B5**) derivative.

We have performed quantum chemical calculations using different levels of theory to be able to make some correlation between the experimental data and the molecular properties of the radicals. As a first step, we compared the spin density at the carbonyl C atom with the different reactivities. It was difficult to make such a correlation because the observed small difference in the reactivity of **B1**-**B5** probably does not arise from a variation in the spin densities.

Usually, it is the interaction between filled orbitals of one reactant with vacant orbitals of the other which leads to a favourable lowering of the energy. In the reaction of a radical with the double bond of the monomer, only the interaction between the SOMO (singly occupied molecular orbital) of the radical and both the HOMO (highest occupied molecular orbital) and LUMO (lowest occupied molecular orbital) are considered. The best energy match between SOMO of the radical and LUMO of the monomer is shown in Figure 3.11.
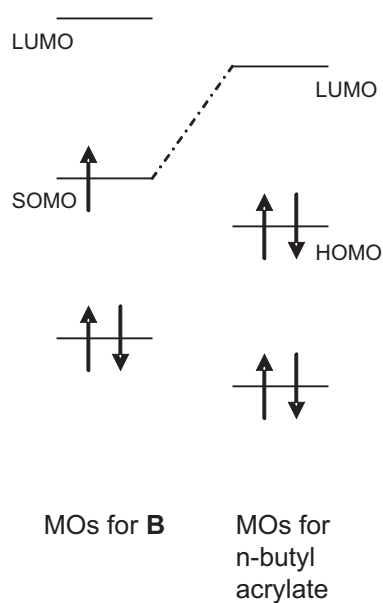
Figure 3.11: The interaction between the SOMO of the radical and the LUMO of the monomer

As a second step, we made a correlation between the reactivity of the radicals **B1**-**B5** towards n-butyl acrylate with the energy gap between the HOMO and LUMO orbitals. The data for this difference and the addition rate constants are shown in Table 3.4.

Table 3.4: Comparison between the addition rate constants of the benzoyl radicals to n-butyl acrylate and the energy gap between the HOMO and LUMO orbitals

Benzoyl Radical	$K_{add}/ .10^6$ mol^{-1}s^{-1}	HOMO – LUMO gap / a.u.
B1	1.18	0.116
B2	1.25	0.101
B3	1.91	0.122
B4	1.25	0.127
B5	1.03	0.117

However, there is no agreement between these calculations and the experimental data. This could be due to the fact, that the steric effects may be important. To model these effects requires more detailed calculations examining the transition state of the reactants.

As a third step we have performed quantum chemical calculations to elucidate the energetics and reaction paths explicitly in regards to the potential energy surfaces profile.

DFT and *ab initio* calculations were carried out using the Gaussian 98 package. All geometries of the radicals and n-butyl acrylate were optimized with B3LYP/6.31G(d). Subsequently, single-point calculations were performed at the obtained geometries, using different methods and a variety of basis sets. The minimum-energy path for the addition reactions were traced by choosing the distance R between the carbon centered radical and the β-carbon atom of the vinyl monomer as the principal reaction coordinate. The transition states (energy saddle points) for the addition reactions were located using Berny algorithm, to evaluate the activation barrier hight.

Correlation of the activation barrier heights calculated for the five carbon centered radicals with their experimental relative reactivity data will be examined.
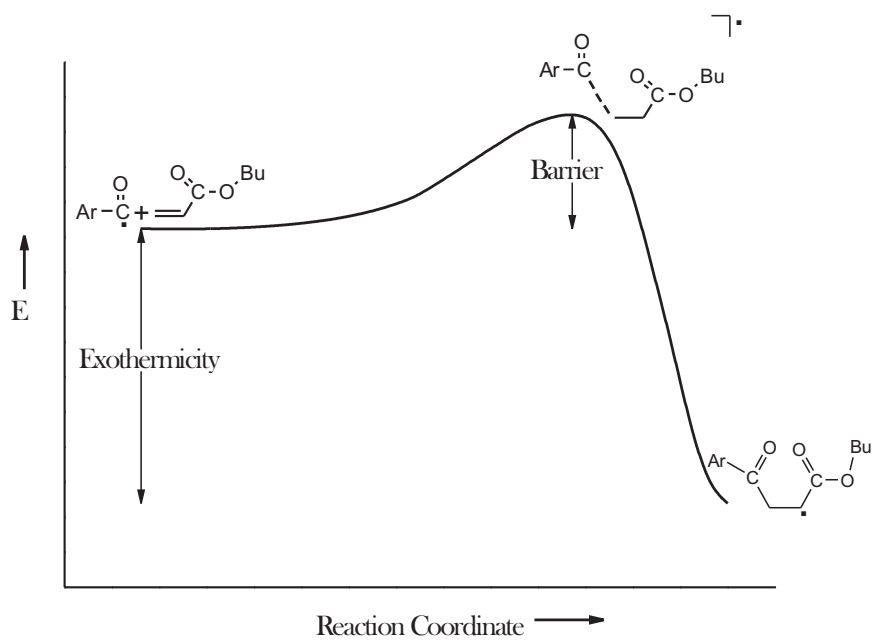
Figure 3.12: Addition reaction of the benzoyl radical to n-butyl acrylate

The schematic potential-energy profile in Figure 3.12 corresponds to the reaction between a radical $R^\bullet$ and n-butyl acrylate, proceeding via a transition structure (TS) to give the product radical. The addition of a reactive carbon-centered radical to a molecule with a multiple carbon-carbon bond is generally exothermic because a π bond is replaced by a σ bond (Figure 3.12). The transition state is early, that is, the cleavage of the π bond and the formation of the σ bond are far from being complete in the transition state.
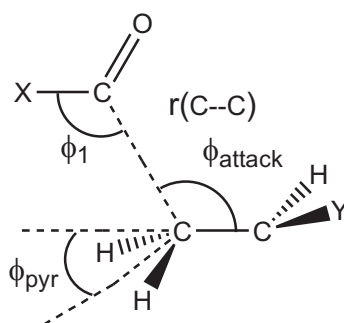
Radical	r(C--C)	F_{attack}	F_1	F_{pyr}
B1	2.351 Å	109.6°	110.5°	11.6°
B2	2.367 Å	103.6°	106.2°	9.7°
B3	2.408 Å	105.4°	118.0°	10.3°
B4	2.407 Å	105.3°	118.0°	10.4°
B5	2.422 Å	105.7°	117.3°	9.8°

Figure 3.13: Transition structures for the addition reaction of the benzoyl radicals **B1**-**B5** to n-butyl acrylate.

B1
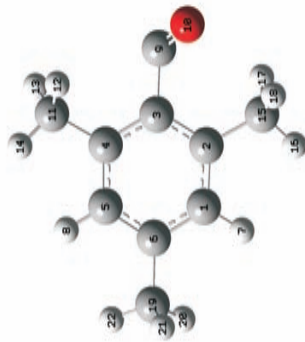
Method	Non-corrected energies		Counterpoise corrected energies		
	Activation Barrier kJ/mol	Exothermicity kJ/mol	Activation Barrier kJ/mol	Exothermicity kJ/mol	BSSE kJ/mol
UHF/6-31G(d)	68.6800	40.3314	76.2025	42.3369	5.76670
B3LYP/6-31G(d)	54.4958	36.5580	64.1245	40.0725	8.32880
B3LYP/6-311G(d)	57.7815	27.1188	63.4555	30.1878	5.90602
B3LYP/6-311G(d,p)	58.5123	24.6683	63.7098	27.7038	5.63433
B3LYP/6-311G(2df,p)	56.7014	25.1695	61.6624	28.0786	5.38965
UMP2/6-31G(d)	194.425	41.4038	212.810	45.8391	13.6279
ROMP2/6-31G(d)	58.4094	51.7127	77.0127	56.1306	13.7196

B2
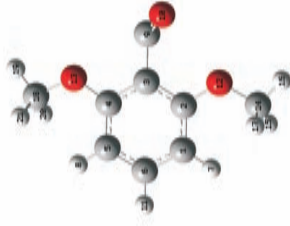
Method	Non-corrected energies		Counterpoise corrected energies		
	Activation Barrier kJ/mol	Exothermicity kJ/mol	Activation Barrier kJ/mol	Exothermicity kJ/mol	BSSE kJ/mol
UHF/6-31G(d)	65.9628	53.9682	73.6466	58.6803	8.55394
B3LYP/6-31G(d)	48.6065	49.3928	46.8823	56.4601	6.20531
B3LYP/6-311G(d)	49.5085	41.8946	56.2424	47.6823	9.15465
B3LYP/6-311G(d,p)	50.1186	39.7369	56.5282	45.4451	8.91309
B3LYP/6-311G(2df,p)	48.8047	39.3054	55.3578	45.0409	9.01204
UMP2/6-31G(d)	157.136	56.9712	174.838	65.6981	17.5780
ROMP2/6-31G(d)	47.2759	61.9791	64.7205	70.7522	17.4955

B3

Method	Non-corrected energies		Counterpoise corrected energies		
	Activation Barrier kJ/mol	Exothermicity kJ/mol	Activation Barrier kJ/mol	Exothermicity kJ/mol	BSSE kJ/mol
UHF/6-31G(d)	43.8991	99.5717	42.1718	109.095	8.66012
B3LYP/6-31G(d)	27.4522	87.6169	13.4571	101.244	6.62944
B3LYP/6-311G(d)	27.4982	80.5473	24.3133	90.0169	7.87719
B3LYP/6-311G(d,p)	28.0362	78.1177	24.5196	87.5228	7.64684
B3LYP/6-311G(2df,p)	28.1916	76.2404	24.4743	85.6022	7.50311
UMP2/6-31G(d)	81.2518	74.5541	81.5543	91.5055	17.1028
ROMP2/6-31G(d)	45.8225	83.1891	46.1936	100.258	17.2543

B4

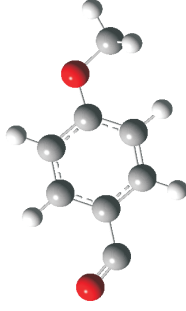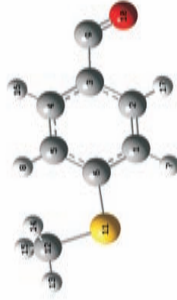| Method	Non-corrected energies		Counterpoise corrected energies		
	Activation Barrier kJ/mol	Exothermicity kJ/mol	Activation Barrier kJ/mol	Exothermicity kJ/mol	BSSE kJ/mol
UHF/6-31G(d)	43.7515	100.866	42.0782	110.197	8.50778
B3LYP/6-31G(d)	27.8851	88.4002	25.1273	101.864	12.0801
B3LYP/6-311G(d)	27.9947	81.2987	24.7797	90.6886	7.77267
B3LYP/6-311G(d,p)	28.5449	78.8781	24.9973	88.1995	7.53789
B3LYP/6-311G(2df,p)	28.6458	77.0462	24.9191	86.3138	7.39556
UMP2/6-31G(d)	82.2186	74.5475	82.5322	91.4183	17.0026
ROMP2/6-31G(d)	46.0587	83.8637	46.4731	100.755	17.0988

B5

| Method | Non-corrected energies | | Counterpoise corrected energies | | |
	Activation Barrier kJ/mol	Exothermicity kJ/mol	Activation Barrier kJ/mol	Exothermicity kJ/mol	BSSE kJ/mol
UHF/6-31G(d)	73.6852	70.2456	79.3115	72.3857	4.95314
B3LYP/6-31G(d)	49.0241	65.5920	56.3421	69.1972	7.26421
B3LYP/6-311G(d)	52.7674	54.6762	55.9115	57.8398	4.73559
B3LYP/6-311G(d,p)	53.2214	52.2137	56.0064	55.3431	4.52187
B3LYP/6-311G(2df,p)	52.0883	51.5272	54.7330	54.5328	4.32801
UMP2/6-31G(d)	95.3071	60.7164	107.865	65.2815	10.8441
ROMP2/6-31G(d)	59.7725	69.5784	72.6589	74.0490	10.9138

Benzoyl Radical	$K_{add}/\ .10^6$ mol^{-1}s^{-1}	Activation barrier [kJ/mol]	Exothermicity [kJ/mol]
B1	1.18	77.0127	56.1306
B2	1.25	64.7205	70.7522
B3	1.91	46.193	100.258
B4	1.25	46.4731	100.755
B5	1.03	72.6589	74.0490

3.1.8   Conclusions

We have shown that TR-EPR is a suitable technique to provide rate constants of addition reactions of benzoyl radicals to alkenes. Two concentration domains of reactivity have been established for the addition of benzoyl radicals to butyl acrylate. At butyl acrylate concentrations below 1.25 M, the corresponding addition constants are between 1.4 and 2.6 10^6 mol^{-1}s^{-1}, as corroborated by TR-EPR measurements at X- and W-band. This is in the same range of values as reported in previous investigations by time resolved infrared spectroscopy. Our experiments demonstrate that the apparent reaction constant of benzoyl radicals decreases at high viscosity. Is this specific for benzoyl radicals or is this a general behavior? This question could be answered by extending these investigations to phosphinoyl and carbon-centered radicals. This, however, is not an easy task since these more reactive radicals are expected to be consumed by the alkene at shorter times, and the transient radicals may escape detection within the time window of TR-EPR experiments. Although the kinematic viscosity of the reaction mixture drastically increases at higher alkene concentrations, no specific line-broadening from slow tumbling motion of the benzoyl radicals is observed. Apparently the increase of macroscopic viscosity of the reaction solution (which slows down the addition reactivity) does not translate into restricted motion of the radicals in their local microenvironment. This unhindered local mobility is corroborated by that fact that the EPR spectra of spin label TEMPO do not reveal any anisotropy over the full viscosity range. Photoinitiators producing benzoyl radicals are occurring in many industrial applications. Hence, their attenuated reactivity towards acrylates at high viscosity has to be borne in mind when estimating the efficiency of the initiating radicals in resins to be applied.

Chapter 4

Oxygen

4.1 Oxygen Inhibition

Light-induced polymerizations offer many advantages over traditional thermal polymerization such as rapid curing, time and spatial control, circumvention of the highly volatile solvents, and low energy consumption. However, one of the greatest limitations to the application of free radical photopolymerization is the inhibitory effect of the oxygen.

Oxygen, either from the air or dissolved in the formulation, may interfere with photopolymerization systems at various stages:

- Ground state oxygen is a triplet state molecule and plays an active role in quenching the excited triplet state of the photoinitiator, thereby preventing the production of primary radicals.

- It can also scavenge the primary radical/propagating radicals to form peroxide radicals which are inactive to initiate polymerization.

The presence of molecular oxygen in photopolymerization system generally introduces an induction period accompanied by the decreased polymerization rate. The ultimate conversion of the system is lowered and the polymer chain length is significantly reduced due to the premature termination of the propagation by oxygen.

Most commercial photoinitiators have very short lived triplet states, thus bimolecular triplet quenching is negligible under most conditions. The main cause for oxygen inhibition with these initiators is not quenching, but the

scavenging of reactive radicals by oxygen at a later stage of the initiation process.

Since the industrial applications of the UV/Vis irradiation curing are under atmospheric conditions, the oxygen presence as from the air as inside the formulations. Therefore, knowledge for the reaction of oxygen towards the initiating radicals is of great importance.

In this project we have been working on a reaction of oxygen towards the phosphorus- and carbon-centered radicals generated from the α-cleavage at the carbonyl-phosphorus bond after the photolysis of **I1** and **I2** initiator solutions. This results in the transformation of highly reactive phosphinoyl- and carbon-centered radicals into less reactive peroxy radicals (Figure 4.1).
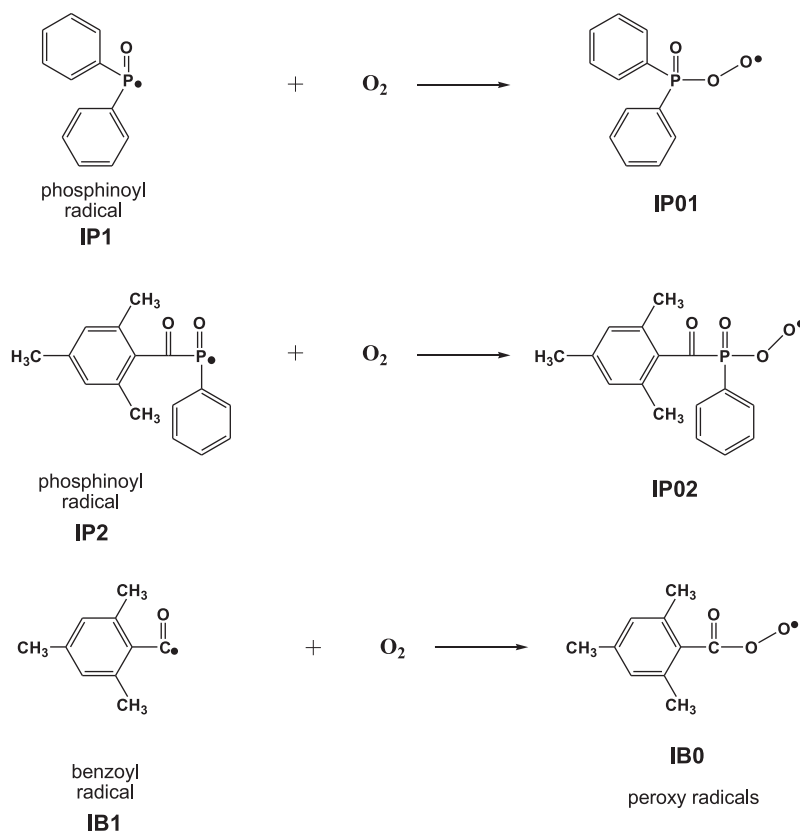
Figure 4.1: Radical scavenging by oxygen.

The reaction of oxygen with the radical initiator leads to line width broadening as in the cases discussed in the previous chapters. Therefore, the kinetic data were extracted from the EPR spectra using the "line width method". The rate constants k_{add} were obtained from the linear plot of the line broadening versus oxygen concentration (see Chapter 2 and Figure 4.2). Variation of the oxygen concentration was achieved by saturation of the toluene solution with oxygen-nitrogen mixtures at 1 atm partial pressure oxygen at 24°C. As expected for such an organic radicals, the rate constants k_{add} range from 2.98 to 6.22×10^{10} $M^{-1}s^{-1}$.
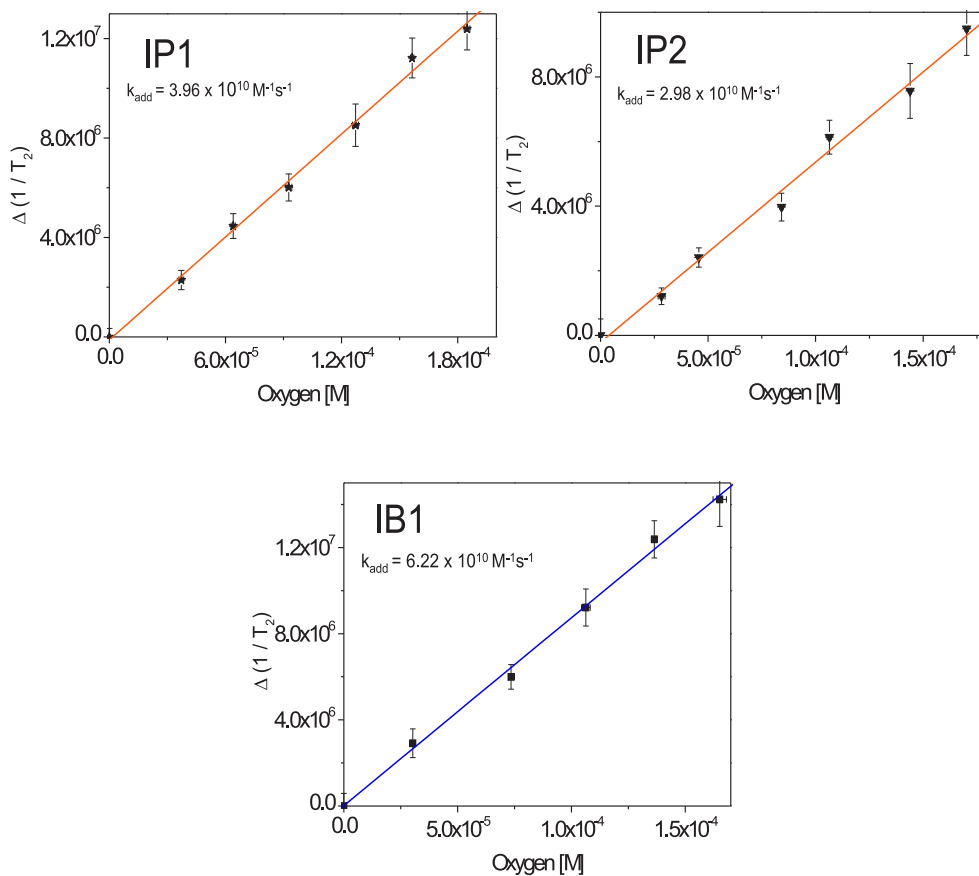
Figure 4.2: Plots of the chemical lifetime *vs.* oxygen concentration for the determination of rate constants k_{add} from TR-EPR spectra at X band for **IP1**, **IP2** and **IB1** radicals.

Although all the addition constants are in the diffusion-control range we can see that k_{add} for the benzoyl radical **IB1** is higher than the one of **IP1** and **IP2**. This result was unexpected since benzoyl radicals have ca. one order of magnitude lower reactivity towards the double bond of the acrylate monomers. Thus, compared to the phosphinoyl radicals, they are less efficient initiators but very efficient oxygen scavengers.

In order to study the whole reaction pathway we performed quantum chemical calculations using density functional theory (DFT) with the B3LYP functional. The attack of oxygen towards **IP1** radical is shown in Figure 4.3.
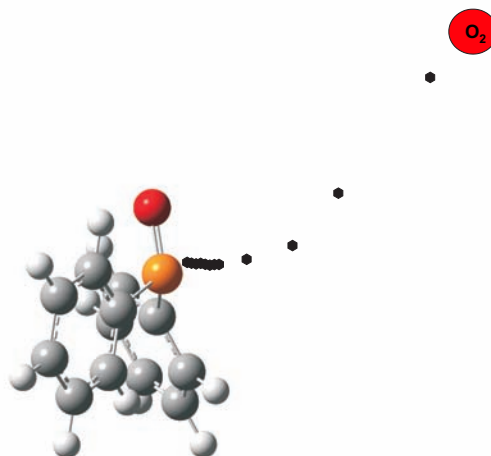
Figure 4.3: The attack of oxygen towards **IP1** radical. Calculations were performed using B3LYP/6-31G* level of theory.

To get some feeling for the different reactivities of the phosphinoyl and benzoyl radicals towards the double bond of n-butyl acrylate and oxygen, on the base of the addition constants obtained from the TR-EPR measurements, we have performed some chemical kinetic simulations in anaerobic conditions (Figure 4.4).

If we first compare the reactions of the two phosphinoyl radicals towards n-butyl acrylate and oxygen in time, we can see not only that the reaction of the two radicals to the oxygen is much faster than the reaction to n-butyl acrylate, but also that the concentration of the oxygen vanishes to zero at about 6×10^{-8} s after the reaction has started. That is why, in the presence of oxygen, both of the radicals predominantly will react to the oxygen. Therefore, the oxygen is an inhibitor of the radical polymerization, since the radicals tend to react with the oxygen and not starting the polymerization process.
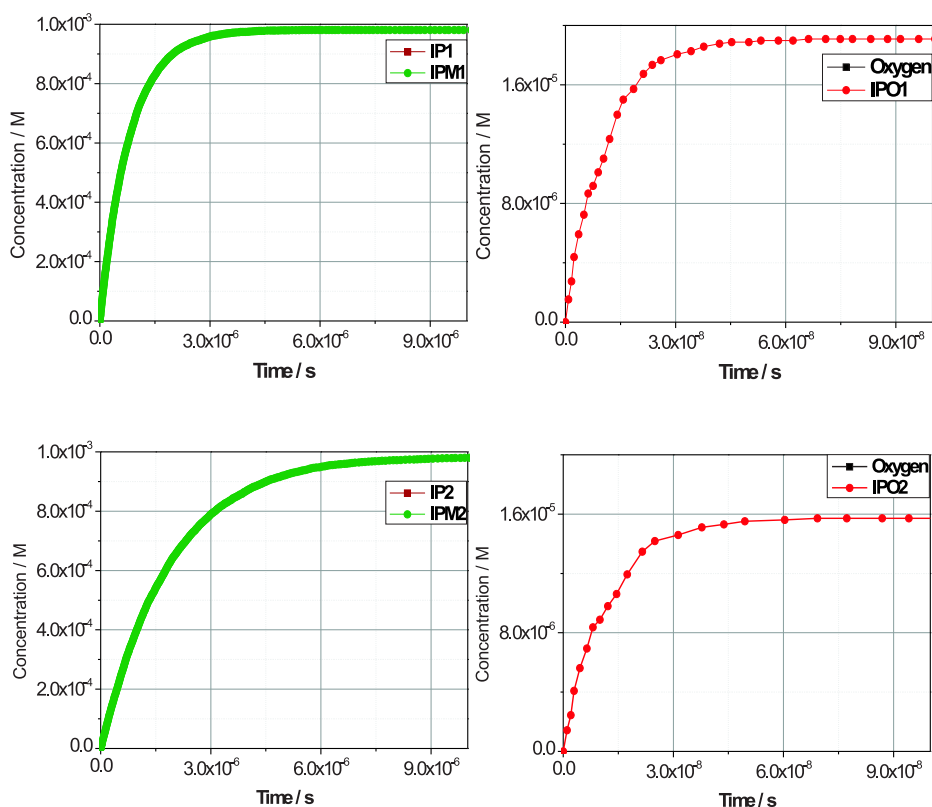
Figure 4.4: Chemical kinetic simulations for the reaction of **IP1** and **IP2** toward n-butyl acrylate and oxygen.

66

The same patten can be seen for the reaction of the benzoyl radical towards oxygen and n-butyl acrylate (Figure 4.5). The reaction with the oxygen molecule is again faster than the reaction with n-butyl acrylate.
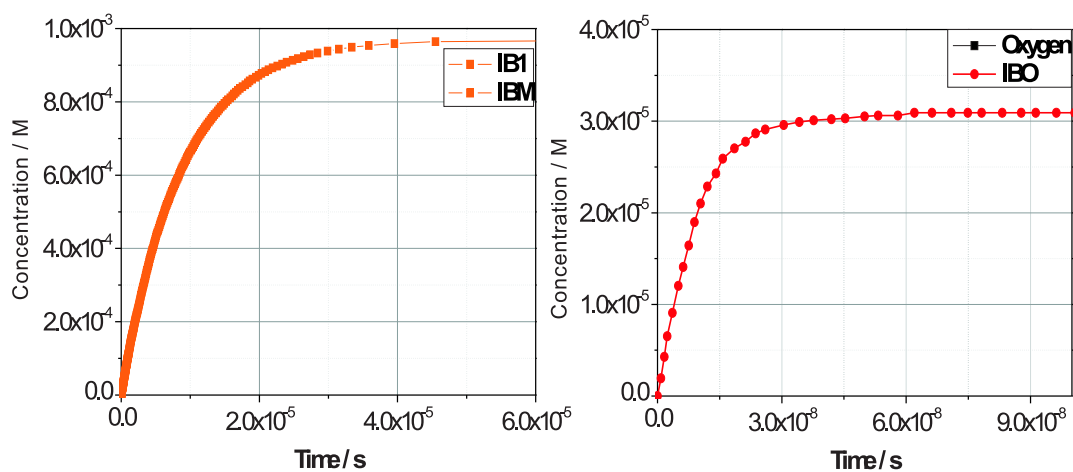
Figure 4.5: Chemical kinetic simulations for the reaction of **IB1** toward n-butyl acrylate and oxygen.

In the previous investigations of the benzoyl and the two phosphinoyl radicals by time-resolved EPR, we have seen that the two phosphorus-centered radicals react by ca. one order of magnitude faster than the carbon-centered radical towards the double bond of the monomer, but in the case of the oxygen they have the opposite patten. If we compare the chemical kinetic simulation data for their reaction towards oxygen, we can see that the oxygen is predominantly consumed from the benzoyl radical (Figure 4.6).
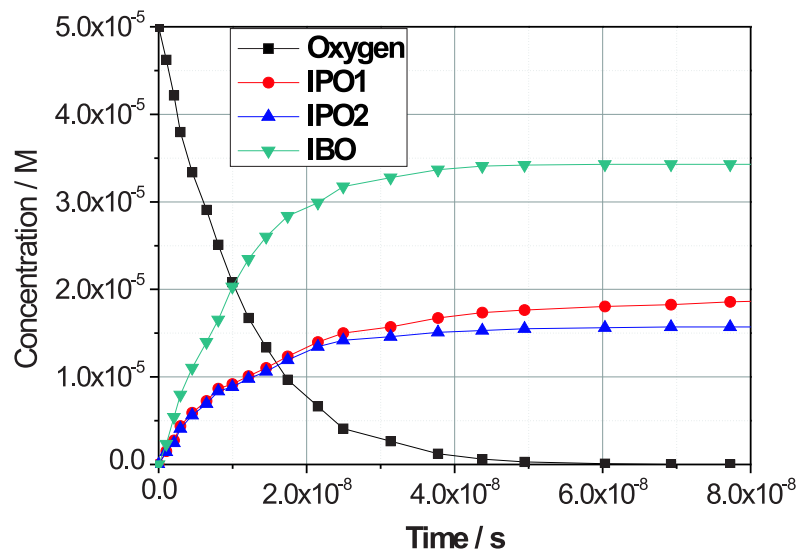
Figure 4.6: Chemical kinetic simulations for the reaction of **IP1**, **IP2** and **IB1** toward oxygen.

Thus, we can conclude that the benzoyl radicals, which are the most often occurring species in the UV/Vis curing systems may not be very efficient initiators of radical polymerization, but they can be used as an oxygen scavenges. This will not only lead to the consumption of the oxygen, but also will increase the efficiency of the phosphinoyl radicals preventing them from their reaction with the oxygen. Therefore, photoinitiators providing high concentration of benzoyl radicals after the homolitic α-cleavage may be of interest.

Chapter 5

Fluorescence

5.1 Fluorescence of the Photoinitiators

UV curing is a dynamic technology with new applications continually being developed. Challenges arise which may include faster speed, improved coating performance or achieving cure under more difficult conditions.

The first stage in any UV curing process is the absorption of a photon from the incident UV energy. For efficient absorption of light and successful photoinduced reactions, the absorbing molecule, i.e. the photoinitiator, must absorb strongly at some of the wavelengths of irradiation and then undergo a transition to an excited state.

Our subject in this work is to answer the questions: Do the photoinitiators have some other property that can be use for the efficient radical polymerization? Do they have fluorescence and can this fluorescence be used as a "light source" for the additional hardening of the coating?

As a beginning of this research, we have started with the investigation of the photochemical properties of the two well know of us and commercially available photoinitiators 2,4,6-trimethylbenzoyl-diphenylphosphine (**I1**) and bis(2,4,6-trimethylbenzoyl)phenylphosphine oxide (**I2**).

As a first step of this investigation we have perform UV/Vis measurements. The ground state absorption spectra of **I1** and **I2** possess absorption maxima at about 280 and 370 nm corresponding to π,π^* and n,π^* transitions respectively. From the emission and excitation spectra recorded in n-hexane solution, it was inferred that the band at 280 nm corresponds to the $S_0 \rightarrow S_1$

transition. Phosphine oxides **I1** and **I2** exhibit broad structureless fluorescence emission at room temperature in n-hexane solution upon 310 and 320 nm excitation respectively. The excitation spectra of **I1** and **I2** are very similar to their UV-VIS absorption spectra. Comparison between the UV-VIS and excitation spectra of **I2** are shown in Figure 5.1. The singlet excited state energy of **I1** and **I2**, estimated from the intersection of the emission and excitation spectra at 380 and 428 nm respectively, are ca. 315 and 279 kJ/mol. Fluorescence emission and absorption spectra obtained with **I1** and **I2** are shown in Figure 5.2.
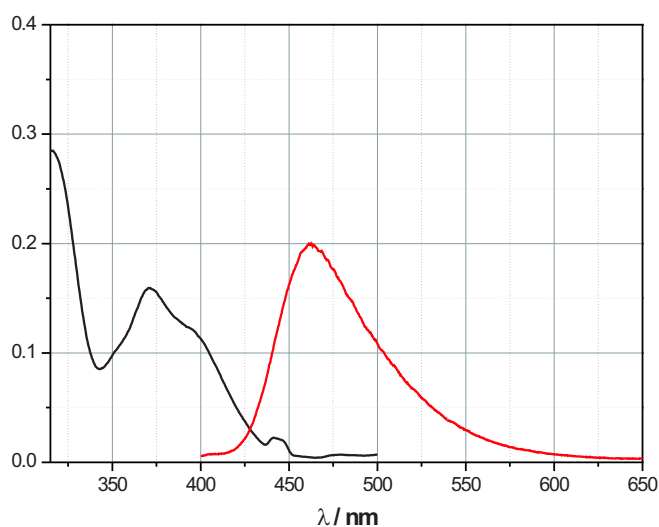
Figure 5.1: Absorption and excitation spectra of **I2** recorded in n-hexane solution at room temperature with an optical path length d of 1 cm. **IP2** = 2.87×10^{-4} mol.l^{-1}.

These measurements showed us that although the fluorescence of both of the initiators is not very strong, it is in the range where most of the initiator molecules have still an absorption. comparison between the absorption and emission spectra of both of the initiator molecules show that the fluorescence emission band intersects the n,π^* absorption band of the photoinitiator **I1** and **I2**. That is why their fluorescence properties can be used to enhance the in depth cure of the formulation. Even more, the fluorescence of the bis(2,4,6-trimethylbenzoyl)phenylphosphine oxide (**I2**) photoinitiator
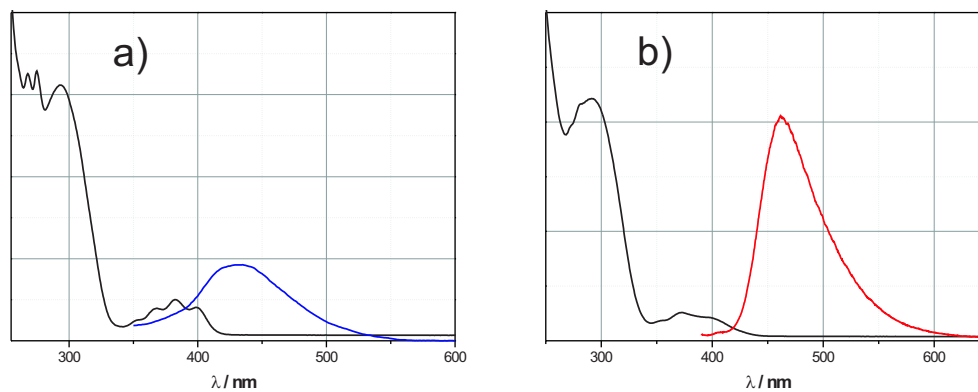
Figure 5.2: Ground state absorption and emission spectra of a) **I1** and b) **I2** recorded in n-hexane solution at room temperature with an optical path length d of 1 cm. **IP1** = 1.56x10^{-4} mol l^{-1} and **IP2** = 2.87x10^{-4} mol l^{-1}.

is slightly stronger than the one of 2,4,6-trimethylbenzoyl-diphenylphosphine oxide (**I1**). This observation allows us to think that triacylphosphine oxide fotoinitiators may have even stronger fluorescence band.

Moreover, measurements in the presence of n-butyl acrylate shows that the intensity of the fluorescence is not influenced by the quencher concentration (Figure 5.3). This has been proven by performing a fluorescence measurements at different concentrations of n-butyl acrylate.
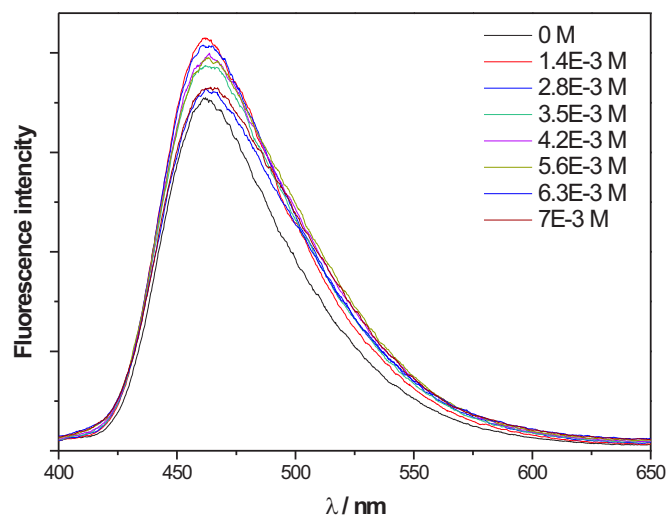
Figure 5.3: Fluorescence emission spectra of **I2** recorded in n-hexane and the presence of different concentrations of n-butyl acrylate. $\lambda_{exc} = 320$ nm; **IP2** $= 2.87 \times 10^{-4}$ mol l^{-1}.

These results confirm our hypothesis, that the photoinitiators **IP1** and **IP2** can be used not only for inducing radical polymerization after the homolitic α-cleavage, but also as a "light source" for curing thick layers. Even more, they can be used as a basis of further investigations. Good candidate for these purposes will be compounds which not only will have a stronger fluorescence, but also there fluorescence band is extended to the shorter wavelength.

Chapter 6

Theoretical Part

6.1 What is Electron Paramagnetic Resonance (EPR)?

6.1.1 Introduction

Electron paramagnetic resonance (EPR), also known as electron spin resonance (ESR) and electron magnetic resonance (EMR), is the name given to the process of resonant absorption of microwave radiation by paramagnetic ions or molecules, with at least one unpaired electron spin, and in the presence of a static magnetic field. EPR was discovered by Zavoisky in 1944. It has a wide range of applications in chemistry, physics, biology, and medicine.

When an atom or molecule with an unpaired electron is placed in a magnetic field, the spin of the unpaired electron can align either in the same direction or in the opposite direction as the field. These two electron alignments have different energies.

The energy differences we study in EPR spectroscopy are due to the interaction of unpaired electrons in the sample with an external magnetic field produced by the EPR spectrometer. This effect is called Zeeman Effect.

6.1.2 The EPR Experiment

Due to its spin, an electron possesses a magnetic moment $\vec{\mu}_e$ given by an expression analogous to Equation 6.1.

$$\vec{\mu}_e = -g\beta\mathbf{S} \tag{6.1}$$

where g is called the g-value ($g_e = 2.00232$ for free electron), μ_B is the Bohr magneton (9.274×10^{-28} JG^{-1}) and $\hbar\mathbf{S}$ is the spin angular momentum vector of the electron.

As it was mentioned before, in the case of a free spin with $M_s = \pm\frac{1}{2}$, only two energy levels are possible and the divergence of the magnetic or Zeeman levels will be linear with field. This is illustrated in Figure 6.1.
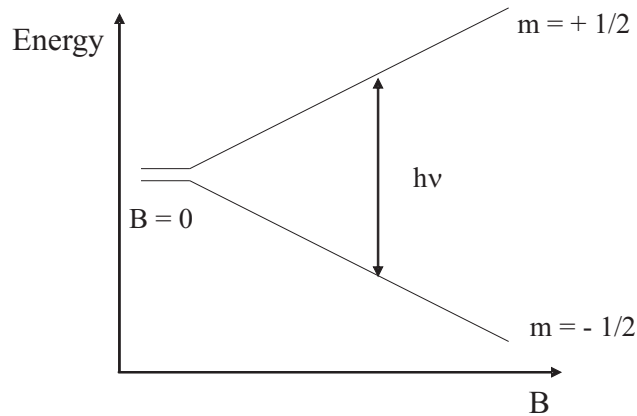
Figure 6.1: Energy levels of an electron placed in a magnetic field.

The corresponding energy levels in a field H_0 are given by (6.2) and the energy differences by equation 6.3.

$$E_{+\frac{1}{2}} = +\frac{1}{2}g\beta H_0, \quad E_{-\frac{1}{2}} = -\frac{1}{2}g\beta H_0 \tag{6.2}$$

$$\Delta E = g\beta H_0 \tag{6.3}$$

Transitions between these levels can be induced by the interaction of electromagnetic radiation of frequency ν such that $\Delta E = h\nu$ and the relation between frequency and field is that given in equation 6.4.

$$h\nu = g\beta H_0 \tag{6.4}$$

The interaction which causes the transitions is between the magnetic dipole of the electron and the oscillating filed accompanying the electromagnetic radiation.

74

6.2 The CIDEP Experiment

6.2.1 Introduction

Whereas classical EPR reflects transitions from energy levels populated according to Boltzmann distribution, EPR spectra at a *ns* time regime exhibit absolute intensities which differ from those of radicals at thermal equilibrium. The experimental effect of those non-equilibrium electron spin populations is called CIDEP (chemically induced dynamic electron polarization) and its mechanisms are discussed below.

The significance of CIDEP is that it provides a direct link between the precise radical observed and the spin multiplicity of the molecule which reacted to form it. If the radicals result from photolysis, this represents an unique connection between the photophysics of the molecule and the subsequent photochemistry of the system under investigation.[53]

There is one serious problem, in time-resolved EPR spectroscopy. For commercial EPR spectrometers, a magnetic field modulation of 100 kHz is routinely used to improve the sensitivity of the spectrometers. The response time of such spectrometers is limited to tens of microseconds. This time-resolution is usually inadequate for the study of photoinduced processes in solution. Two methods have been devised for the improvement of the response time, eliminating the field modulation with a loss of signal sensitivity.[54, 55]

The first method is the direct CW (continuous wave) detection and the second is the pulsed microwave electron spin-echo or Fourier transform method. The time-resolution reachable with the first method is about 50 ns and with the second one about 10 ns.

Although, the sensitivity of the TR-EPR spectrometers is much lower than that of the conventional ones, the discovery of extremely large anomalies in the EPR intensities of many transient radicals has improved the sensitivity of their detection.[56]

6.2.2 Spin Polarization

The magnitude of spin polarization is defined as the ratio of the difference in the populations of the electron spin states to their sum. It is defined as follows:

$$P=(n_\alpha\text{-}n_\beta)/(n_\alpha+n_\beta)$$

where n_α and n_β are the populations of the upper- and lower-spin states, respectively. In CIDEP, the spin polarization |P| typically becomes hundreds times as large as the equilibrium polarization at room temperature $|P_{eq}|$. The equilibrium value, serves as a reference. The intensity of a transition in a CIDEP spectrum is proportional to the product of the concentration of the radical and the appropriate polarization factor, with the degeneracy taken into account, and is not a direct measure of radical concentration. Figure 6.2 shows the cases of emission (P>0) and enhanced absorption (P<P_{eq}) in CIDEP.
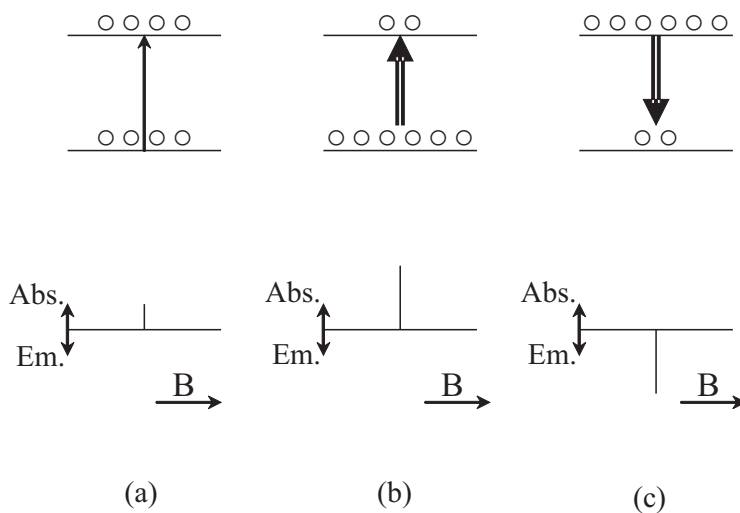
Figure 6.2: EPR signals observed at the situation of (a) thermal equilibrium, (b) enhanced absorption, and (c) emission.

In solution such anomalous polarizations arise from two mechanisms: the triplet mechanism (TM) and radical pair mechanism (RPM). Although the TM and RPM may occur independently in the same reaction system, the actual CIDEP spectra often have contributions due to both the TM and RPM.[57, 58]

6.2.3 Triplet Mechanism (TM)

It is possible for the triplet mechanism to appear in reactions which proceed through triplet-excited states. Initially, the precursor molecule is in a singlet state S. Then it is photoexcited to an excited singlet state S* from which there is intersystem crossing (ISC) into the triplet state. If the triplet reacts to form free radicals before its polarization is removed by rapid spin-lattice relaxation, spin-conservation in the reaction step produces spin-polarized radicals, with equilibrated polarization magnitudes.
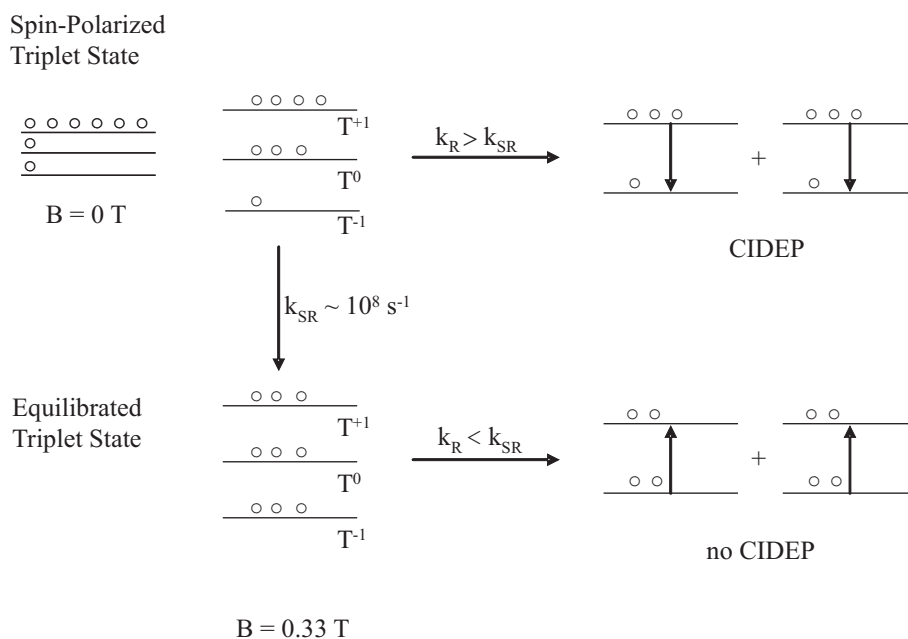
Figure 6.3: The TM for CIDEP of two radicals produced from a spin-polarized triplet state.

Conditions for the appearance of TM are given as follows:

- Reaction should occur from a triplet precursor where spin-polarization is generated through the selective ISC from the lowest singlet state to the triplet one.

- Magnetic field and molecular rotation should not be too extensive to smooth away the spin-polarization in the lowest triplet state.

- Reaction should occur from such a spin-polarized triplet state before its spin-relaxation.

The CIDEP due to the TM has either a totally emissive or absorptive phase pattern and the relative intensities of its hyperfine lines are not distorted from those observed for radicals at thermal equilibrium. TR-EPR spectrum of two radicals produced from a spin-polarized triplet state is shown in Figure 6.4.
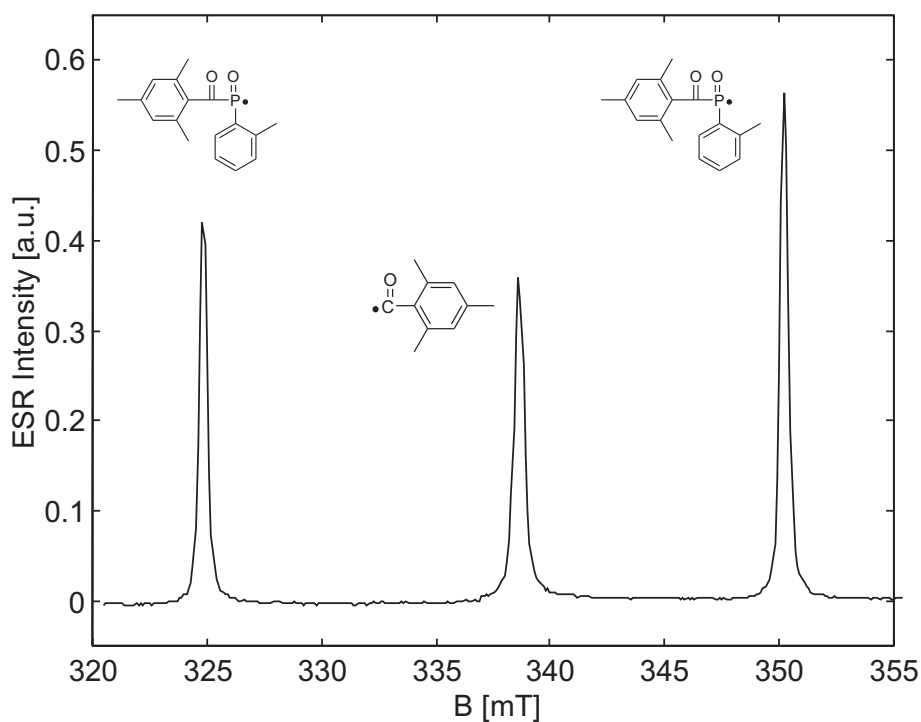
Figure 6.4: The TR-EPR spectrum of bisacylphosphin oxide photoinitiator observed 200-300 ns after the laser flesh (355 nm). Phosphinoyl radicals are TM-polarized.

6.2.4   Radical Pair Mechanism (RPM)

In many photoinduced and radiation-induced reactions, radical pairs (RP) are produced at their initial stage through decomposition, electron transfer, and hydrogen abstraction. Because of spin-conservation rule, a singlet RP (^{1}RP) consisting of two radicals ($R^{1\bullet}$ and $R^{2\bullet}$) is produced from a singlet precursor (^{1}RP) and a triplet RP (^{3}RP) from a triplet precursor (^{3}RP).[59]

Figure 6.5 shows the distance (r) dependence of the energies of (^{1}RP) and (^{3}RP) in the presence of a magnetic field. This figure shows that the singlet S (^{1}RP) and the ^{0}T sub-level of (^{3}RP) reach the same energy at large distances and that S (^{1}RP) and T^{-1} of (^{3}RP) cross at (r_{LC}).

These S-T^0 and S-T^{-1} mixings bring about not only CIDEP but also chemically induced dynamic nuclear polarization (CIDNP) and magnetic field effects on chemical reactions (MFECR). The mechanism producing CIDEP, CIDNP and MFECR is called RPM.
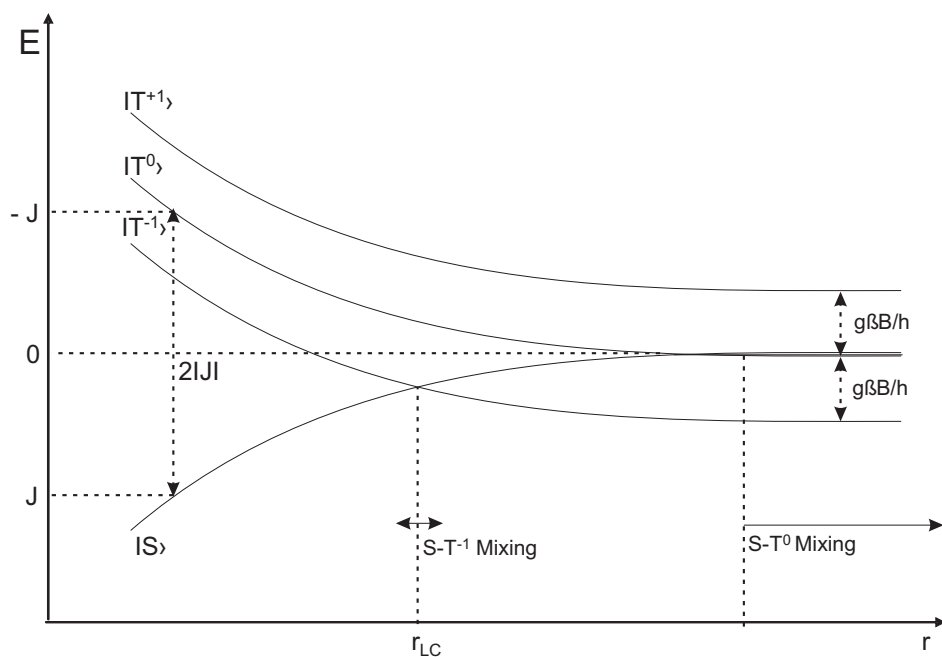
Figure 6.5: Schematic diagram showing the distance dependence of the energy of the singlet and triplet states of a radical pair in the presence of a magnetic field.
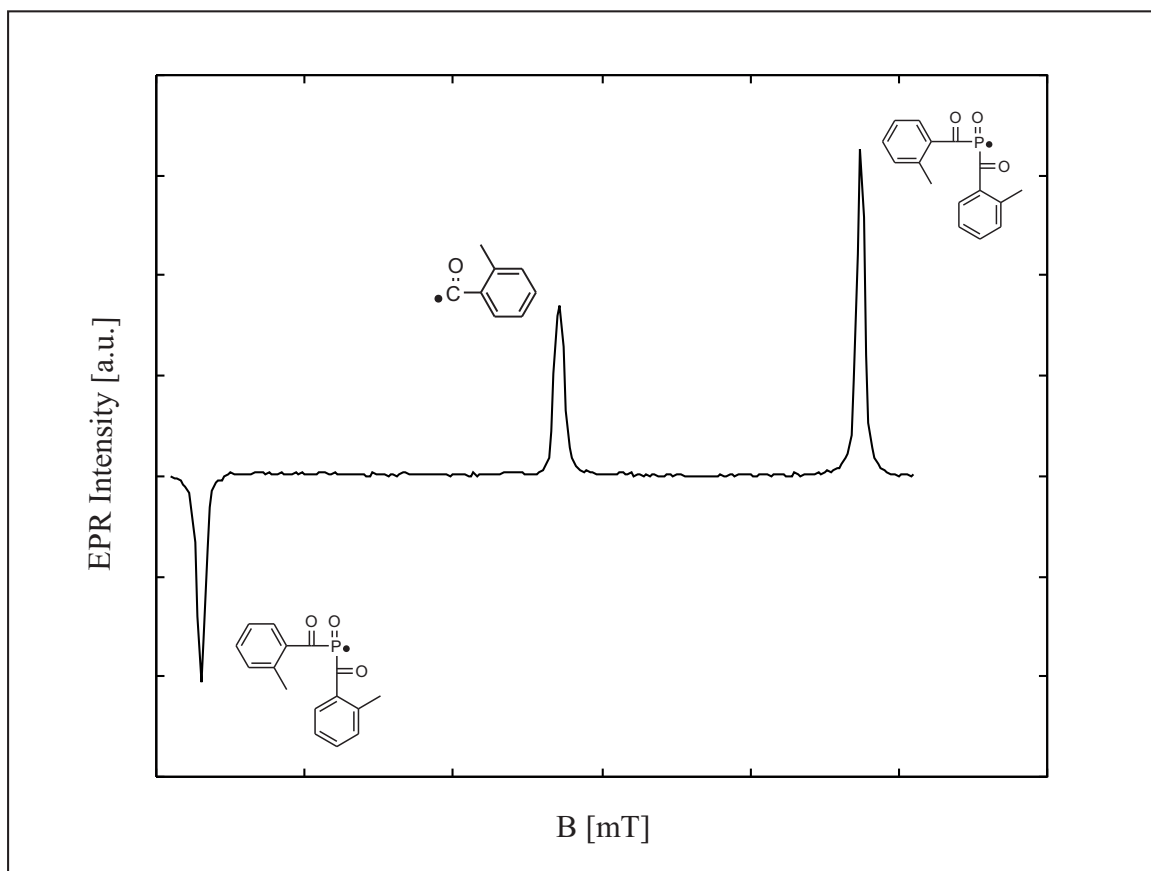
Figure 6.6: The TR-EPR spectrum of phosphinoyl and benzoyl radicals observed 200-300 ns after the laser flash (355 nm). Example of RPM.

The ST_0 Radical Pair Mechanism (RPM)

At the magnetic field of an EPR spectrometer, and in liquid solutions, it is only the S and T_0 states of the spin correlated radical pair that are mixed, since the $T_{\pm 1}$ ones are separated from them in energy by the Zeeman interaction by an amount that exceeds the mixing interaction.

The current theory of polarization of free radicals requires that a pair must first encounter, then separate to a distance for which the value of the electron exchange interaction (J) is near zero, and then return to form a colliding pair. The polarization selection occurs upon radical reencounter under the influence of J. The creation of electron spin polarization through the RPM

depends upon the subsequent action of the electron exchange interaction J, which accumulates more up (α) spin in one radical and more down (β) spins in the other radical. Experimentally, the mixing of some hyperfine states of the radicals usually exhibits an excess of absorption (A); other hyperfine states exhibit an emission (E).

If the radicals are of similar type with similar g-values, e.g. both are carbon-centered radicals, each exhibits a spectrum with some lines in emission (E) and some lines in absorption (A). If the singlet state of the radical pair lies below the triplet one, a spectrum in which the low field lines are in emission and the high field ones are in absorption demonstrates that the radicals were formed by reaction of a triplet molecular state. Radicals from singlet precursors exhibit A/E patterns if $J(r)$ is negative.

Besides causing phase inversions between the two halves of the spectrum, ST_0 RPM affects the relative intensity of the lines, which differ from those of equilibrated radicals. They are determined by the extent of spin mixing which occurs as one radical in a given hyperfine state encounters a second in a different one.

The ST_{-1} Radical Pair Mechanism (RPM)

In systems of neutral radicals, with $J(r)$ negative, the T_{-1} Zeeman sublevel of the radical pair crosses the S one whilst $J(r)$ falls as the radicals diffuse apart. This normally happens too quickly for the efficient generation of ST_{-1} polarization. Exceptions occur when unusually large hyperfine coupling exist (for example in P-centered radicals), when diffusion is inhibited at high viscosity or by confining the radical pair inside micelles.

6.3   Relaxation Times. Bloch Equations.

A general and comprehensive treatment of relaxation processes and line widths would necessitate consideration of:

- the interaction of each electronic dipole with all other electronic and nuclear dipoles in the sample and with the surrounding diamagnetic molecules

- the effect of vibrational, rotational and translational motion of these species and of electron exchange between them

- chemical reactions of the paramagnetic species.

All these interactions can increase the line width by decreasing the lifetime of the spin state undergoing the observed transition, or by changing the magnetic field experienced by the spin at the instant of the transition. Line broadening may also be caused by unresolved nuclear hyperfine structure, by an inhomogeneous magnetic field or variations in the frequency of the oscillating field.

Felix Bloch introduced in a phenomenological way two relaxation rates $1/T_1$ and $1/T_2$. T_1 is called longitudinal relaxation time and T_2 transverse relaxation time. T_1 implies interaction between the 'spin system', i.e. the species with the unpaired electrons, and the surrounding molecules, known as the 'lattice'. T_2 characterize the spin-spin interactions. The introduction of this two relaxation terms assures, that the magnetization M returns to the thermal equilibrium case in exponential decays.

Besides providing a clear description of T_1 and T_2 Bloch's equations give a very satisfying macroscopic explanation of magnetic resonance absorption and predict a definite kind of line shape.

The Bloch equations for the bulk magnetic moment $\mathbf{M}$ including the effect of relaxation and Larmor procession are:

$$\frac{dM_x}{dt} = \omega_0 M_y - \frac{M_x}{T_2} \tag{6.5}$$

$$\frac{dM_y}{dt} = \omega_0 M_x - \frac{M_y}{T_2} \tag{6.6}$$

$$\frac{dM_z}{dt} = -\frac{(M_z - M_0)}{T_1} \tag{6.7}$$

In a magnetic resonance experiment the total applied magnetic field is made up of a steady component in the z-direction, and a rotating component in the xy-plane. Under these conditions the Bloch equations of motion for a collection of electron spins are:

$$\frac{dM_x}{dt} = \gamma(-M_\mathbf{y} H_\mathbf{0} + M_\mathbf{z} H_\mathbf{1} \sin \omega t) - \frac{M_x}{T_2} \tag{6.8}$$

$$\frac{dM_y}{dt} = \gamma(-M_\mathbf{z} H_\mathbf{1} \cos \omega t + M_\mathbf{x} H_\mathbf{0}) - \frac{M_y}{T_2} \tag{6.9}$$

$$\frac{dM_z}{dt} = \gamma(-M_{\mathbf{x}}H_{\mathbf{1}}\sin\omega t + M_{\mathbf{y}}H_{\mathbf{1}}\cos\omega t) + \frac{M_0 - M_z}{T_1} \tag{6.10}$$

The spin performs a damped precession in which the rotating transverse components of $\mathbf{M}$ decay to zero with a characteristic time T_2, while M_z relaxes towards its equilibrium value M_0 with a decay time T_1.

The Bloch equations have been generalized to account for chemical reactions and polarization productions. The resulting equations are:

$$d\vec{M}/dt = \bar{L}\vec{M}(t) - T_c^{-1}(t)\vec{M}(t) + \vec{F}(t) \tag{6.11}$$

where

$$\bar{L} = \begin{pmatrix} -T_2^{-1} & \triangle\omega & 0 \\ -\triangle\omega & -T_2^{-1} & -\omega_1 \\ 0 & \omega_1 & -T_2^{-1} \end{pmatrix} \tag{6.12}$$

$$\vec{F}(t) = \begin{pmatrix} 0 \\ 0 \\ f_a(t) \end{pmatrix} \tag{6.13}$$

and

$$f_a(t) = P_{eq}T_1^{-1}n(t) + P_a(I)k_0(t) + P_a k_2 F n_B(t)n(t) \tag{6.14}$$

The first terms on the right-hand side in Equation 6.11 describes the time dependence due to the interactions with the magnetic fields and due to spin relaxation. The second term is a relaxation term describing the lifetime broadening caused by the chemical reaction of the radicals; the instantaneous chemical lifetime $T_c(t)$ is defined as the reciprocal of the relative rate of radical disappearance - $n(t)^{-1}$ dn/dt. The last term in Equation 6.11 contains contributions from the three polarization terms defined in Equation 6.14.

The first term in Equation 6.14 expresses that the z-component of magnetization relaxes toward the instantaneous "equilibrium" magnetization $P_{eq}n(t)$; n(t) is the instantaneous number of the investigated radical in the sample.

The second term in Equation 6.14 represents an initial polarization production; $k_0(t)$ is the rate of formation of the radicals and $P_a(I)$ is the initial polarization of the radical in hyperfine state a. This initial polarization may be due to the triplet mechanism as well as to the radical pair mechanism.

The last term in Equation 6.14 represents the polarization production resulting from a termination reaction.

Analysis of equations 6.11 and 6.14 show that the transverse relaxation time T_2 is not influenced by the polarization term, which involves the magnetic moment in z-direction. Also, the chemical lifetime $T_c(t)$ for a first-order process is time independent. Neglecting for a moment the chemically induced polarization and chemical reactions, from equation 6.11 we obtain:

$$d\vec{M}/dt = \begin{pmatrix} -T_{2c}^{-1} & \triangle\omega & 0 \\ -\triangle\omega & -T_{2c}^{-1} & -\gamma B_1 \\ 0 & \gamma B_1 & -T_{1c}^{-1} \end{pmatrix} \vec{M}(t) + T_1^{-1}nP_{eq} \qquad (6.15)$$

where

$$T_{2c}^{-1} = T_2^{-1} + T_c^{-1} \qquad (6.16)$$

By Laplace transformation of Equation 6.15, for low value of the alternating field we obtain:

$$u(\omega) = M_0\gamma B_1 \frac{\triangle\omega}{T_{2c}^{-2} + (\triangle\omega)^2} \qquad (6.17)$$

$$\omega(\omega) = M_0\gamma B_1 \frac{T_{2c}^{-1}}{T_{2c}^{-2} + (\triangle\omega)^2} \qquad (6.18)$$

$$M_z = M_0 = nP_{eq} \qquad (6.19)$$

where u and ω are the components of magnetization $\vec{M}$ in rf-frame and M_0 is the initial magnetization. From Equation 6.18 it can be seen that the line shape, characterized by T_{2c}^{-1}, is not affected by the polarization term (Equation 6.14).

Chapter 7

Experimental Part

7.1 Experimental Methods

7.1.1 CW TR-ESR Experiment

Description of the equipment

For the measurements of a time-resolved continuous wave (TR-CW) EPR, a Bruker spectrometer ESP 300E equipped with a microwave amplifier and a TE_{102} microwave cavity (microwave power 9 mW, response time 40 ns) was operated without field modulation. Radicals possessing electron spin polarization are produced in the cavity of the spectrometer by a short laser pulse, and the EPR transitions are observed with nanosecond time resolution in a fixed external magnetic field B_0. The resonance of the EPR spectrometer after a light pulse at a precise, fixed value of the static magnetic field was stored in a Le Croy 9400 dual 125 MHz digital oscilloscope. This is output to a computer with a Debian Linux operating system and equipped with a GPIB interface board. The experiment is controlled by the program $fsc2$ written by J. T. Törring (Institute for Experimental Physic, Free University Berlin). A block diagram of the time-resolved EPR experiment is shown in Figure 7.1.
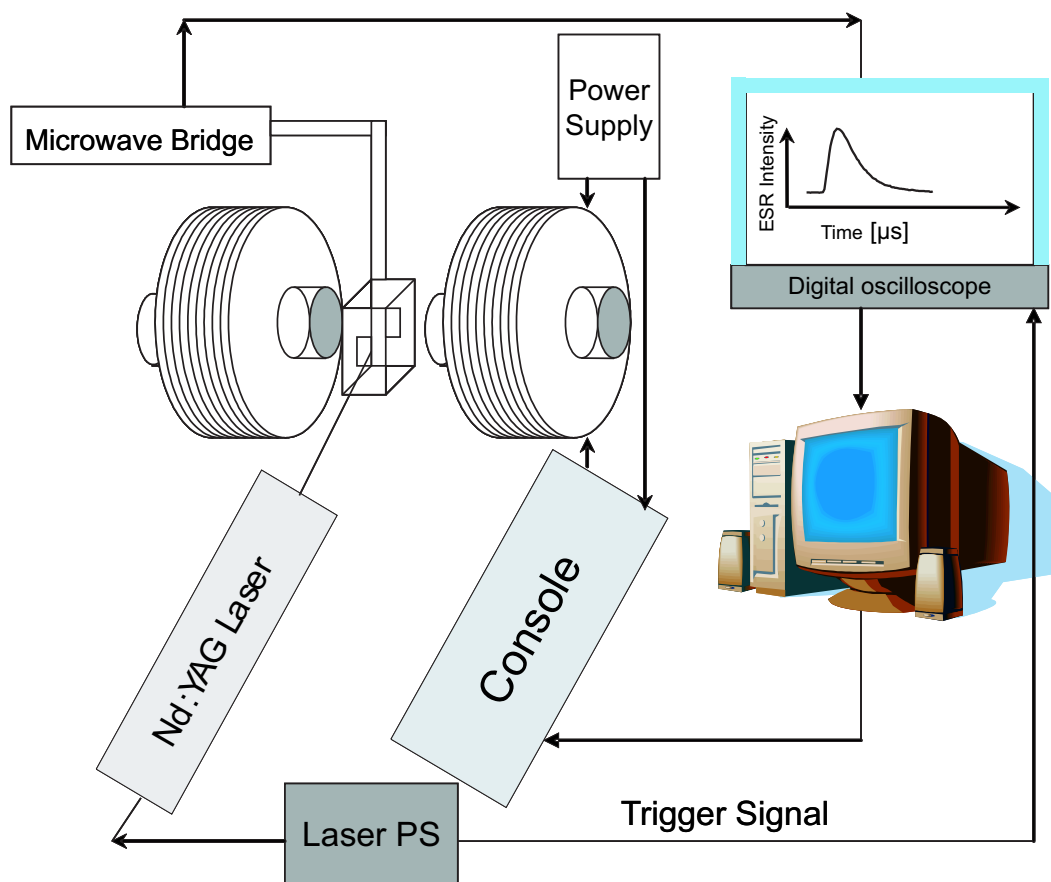
Figure 7.1: Block diagram of the time-resolved EPR spectrometer.

A *ContinuumSureliteII* Nd:YAG laser was used as irradiation source. The excitation wavelength was 355 nm, with flash repetition frequency of 20 Hz and pulse width 4-6 ns. The advantage of using 355 nm wavelength is that it is absorbed by many photochemically active chromophores, but not by common solvents.

The freshly prepared sample solutions in toluene were degassed with argon and pumped through the cavity using a home-build flow system, providing fast, turbulent flow in order to obtain optimum mixing. To avoid distortions of the ESR signals due to the solution flow a constant flow rate was kept and attention was paid to suppress the appearance of gas bubbles in the sample volume. The measurements were performed at room temperature.

The timing sequence for the time-resolved EPR experiment is shown in Figure 7.2.
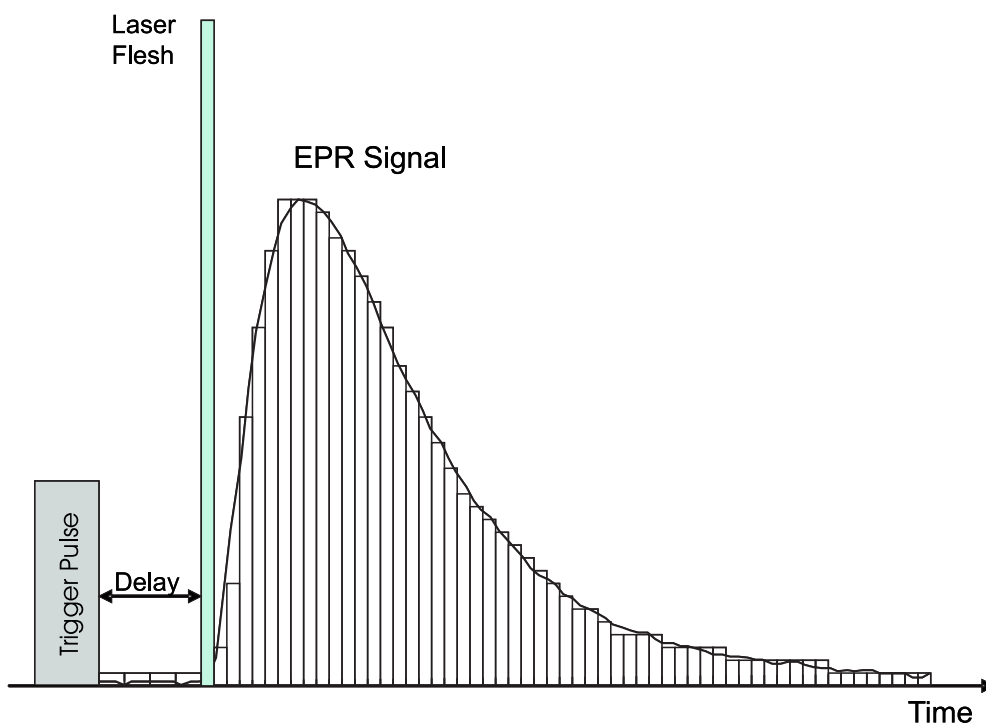
Figure 7.2: The timing sequence for the time-resolved EPR experiment.

To obtain an entire spectrum, the external magnetic field is varied incrementally and the measurements are repeated a number of times and averaged to obtain an acceptable level of signal-to-noise ratio. The data of the experiment in the chosen field region consist of a matrix of intensity versus time. An example of TR-EPR spectrum for the phosphorus- and carbon-centered radicals produced by photolysis of bis(2,4,6-trimethylbenzoyl) phenylphosphine oxide is shown in Figure 7.3.
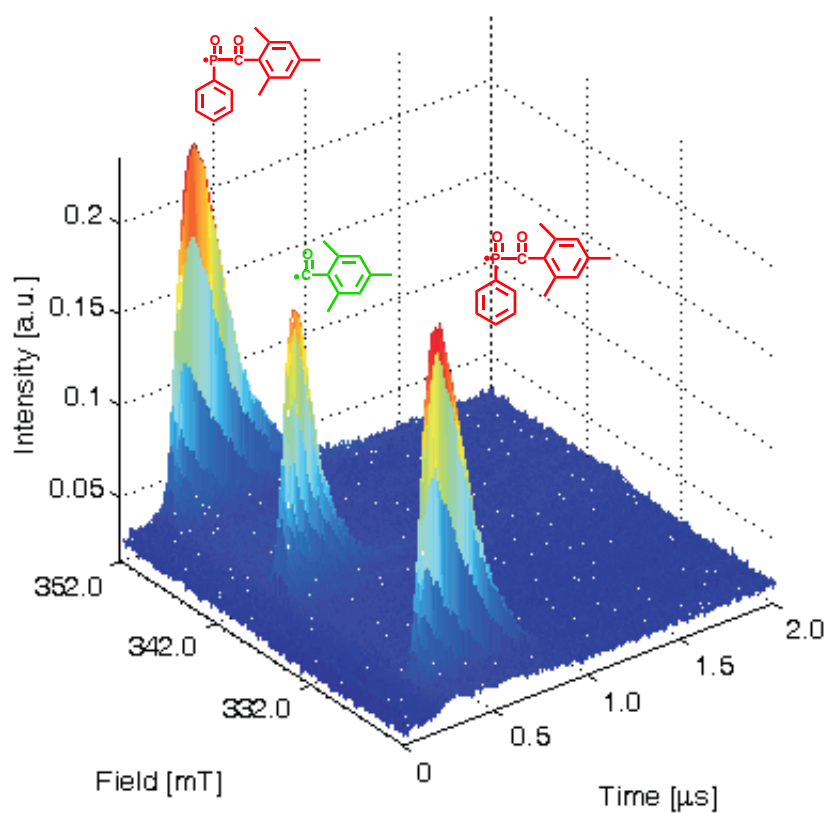
Figure 7.3: TR-EPR spectrum for the phosphorus- and carbon-centered radicals produced by photolysis of bis(2,4,6-trimethylbenzoyl)phenylphosphine oxide.

Sample Preparation

The photoinitiators were provided by Ciba Specialty Chemicals and used without further purification. The compounds were dissolved in toluene (0.005-

0.01 M), and the solutions were saturated with argon. n-Butyl acrylate (Fluka purum) was used in concentrations which varied between 0.3 and 2.8 M. Styrene (Aldrich purum) was used in concentrations between 0.1 and 0.4 M. 1-vynil-2-pyrrolidon (Aldrich purum) was used in concentrations between 0.2 and 1 M and hexamethylendiol-diacrylate (HDDA) (provided by Ciba Specialty Chemicals) was used in concentrations between 0.2 and 0.6 M.

Viscosity Measurements

Figure 7.4: Ubbelohde viscometer.

Solutions of identical concentrations of the photoinitiator in toluene and different concentrations of n-butyl acrylate were first used for TR-EPR measurements and then the viscosity was measured by means of a capillary Ubbelohde viscometer thermostated at 20°C. The viscometer was obtained from Schott Gerte, with instrumental constant: K(0C, 0,5-3cSt) = 0,003164 mm^2/s^2. The time needed for the solution to pass through the capillary multiplied by this constant gives the kinematic viscosity of the probe. Knowing the kinematic viscosity and the density we can find the dynamic viscosity ($\nu = \eta/\rho$). All the measurements were repeated at least ten times.

7.1.2 Fluorescence Measurements

Solutions of identical concentrations of the photoinitiator with different concentrations of n-butyl acrylate were prepared in such a way that the photoinitiator optical density at the excitation wavelength was always smaller than 0.3 (optical path length d of 1 cm), to prevent any re-absorption or inner filter effects that distort the emission spectra. The excitation wavelength was 310 nm in the case of 2,4,6-trimethylbenzoyl-diphenylphosphine oxide **I1** and 320 nm in the case of bis(2,4,6-trimethylbenzoyl)phenylphosphine oxide **I2**, in order to avoid the appearance of Raleigh and Raman scattering. Therefore, the concentration of the photoinitiator was never higher than 10^{-5} M, and much smaller than the concentration of the monomer. Absorption spectra of all the samples were always acquired to correct any deviations in the photoinitiator concentration within a set of measurements. The fluorescence spectra were not corrected. All the measurements were done at room temperature.

Absorption spectra were obtained using Shimadzu UV-3101PC double beam scanning spectrometer with slits for a final resolution of 2 nm. The fluorescence measurements were done on ISA FluoroMax-2 fluorometer, with excitation and emission slits of 2 nm.

Analysis of the fluorescence dater were performed with the help of commercial software (Origin^{TM} version 7.5).

7.1.3 Oxygen Measurements
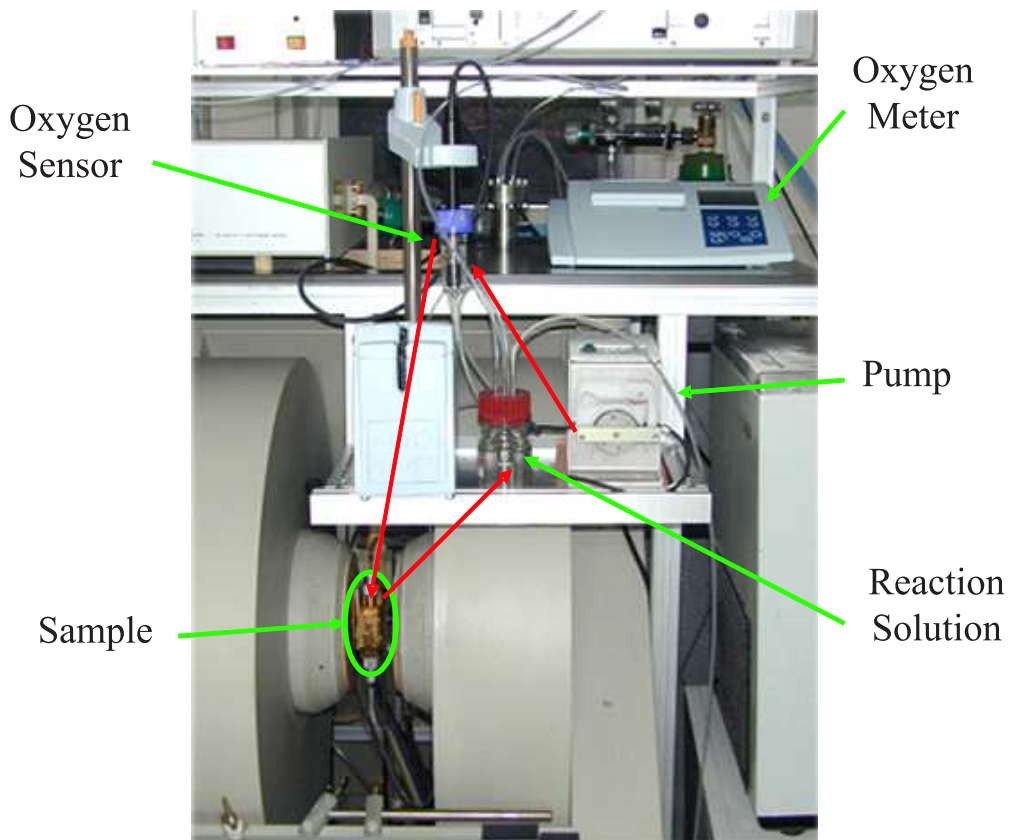
Figure 7.5: Experimental set up for the oxygen measurements.

The compact *inoLab Oxi Level* 2 dissolved oxygen meter allows us to perform rapid and reliable dissolved oxygen measurements. The oxygen sensor *CellOx* 325 was placed in a flow chamber which was connected to the flow system of the TR-EPR measurement. This gave us the possibility to measure the oxygen concentration during to TR-EPR measurement. The specifications of the dissolved oxygen meter are presented in Table 7.1.

Table 7.1: Specification of the Oxygen Sensor.

	Range	Resolution	Accuracy
mg/l	0 ... 19.99	0.01	± 0.5 %
T [°C]	0.0 ... 50.0	0.1	< 2 %

7.1.4 Quantum Chemical Calculations

All of the calculations were performed with the Gaussian 98 series of programs. Different methods were used: DFT (B3LYP), Hartree-Fock (HF) and Möller-Plasset perturbation (MP2). Minimum energy structures were fully optimized with B3LYP/6.31G(d). Subsequently, single-point calculations were performed at the obtained geometries, using different methods and a variety of basis sets. The minimum-energy path for the addition reactions were traced by choosing the distance R between the β-carbon atom of the n-butyl acrylate as the principle reaction coordinate. The transition states (energy saddle points) for the addition radicals were located, using Berny algorithm, to evaluate the activation barrier hight. Basis set superposition error was calculated using counterpoise procedure. At a given level of theory the activation barrier was calculated as the electronic energies difference between the saddle point and the minimum structures.

7.1.5 Software

We have used program written in Matlab code for simulation of the TR-EPR spectra. Matlab is an interactive program system copyrighted by The Mathworks, Ins., Cochituate Place, 24 Prime Park Way, Natick, MA 01760.

To calculate the line width of the TR-EPR signal for a defined time interval we have used a script called $lw10.m$.

```
function [] = lw10(b,t,ytt,p,k)
clc; clf; hold off
idf = input(",'s');
if isempty(idf), idf = ("); end
```

```
disp('')
disp('Please press any key.')  pause

disp('')
disp('Please stand by... Calculations in progress...')
disp('')
format short

ds=ytt; [r,c] = size(ds);
noisd=ones(r,1)*((ds(10,:)+ds(11,:)+ds(7,:)+ds(8,:)+ds(9,:))/5);
ds=ds-noisd; ytt=ds;

be=length(b);
te=length(t);
op=[0];

ymax=max(ytt');
ytm=ymax./max(ymax);
for i=1:be-1
if ytm(i)==1; b0=b(i); mmm=i; end
end

x0=[b0 0.0 0.20 0.10]

if k==0
yt=ytt(:,p)./norm(ytt(:,p),inf);
y = y1(x0,b);
plot(x0(1)-b,y,'g',x0(1)-b,yt,'r',x0(1)-b,ytm,'b')
ylabel('ESR Intensity [a.u.]')
xlabel('B [mT]')

disp('')
disp('Please press any key.')
pause

for i=1:9 [x1]=fminsearch(@ga,x0,[optimset],b,yt);
x0=x1;
y=y1(x0,b);

hold on
plot(x0(1)-b,y,'g',x0(1)-b,yt,'r')
```

```matlab
ylabel('ESR Intensity [a.u.]')
xlabel('B [mT]')

end

sig=std((yt-y))
abs(x0)

else
for j=1:k-p+1,
yt=ytt(:,p+j-1)./norm(ytt(:,p+j-1),inf);

for i=1:9 [x1]=fminsearch(@ga,x0,[optimset],b,yt);
x0=x1;
end

y=y1(x0,b);

sig=std((yt-y));
d(j,:)=[sig abs(x0)];
end

disp('')
d(:,5:5)

clf;
plot(x0(1)-b,y,'g',x0(1)-b,yt,'r')
hold on
ylabel('ESR Intensity [a.u.]')
xlabel('B [mT]')
title(idf)

disp('')
disp('Please press any key.')
pause

clf;

errorbar(t(p+1:k+1),d(:,5),d(:,1),d(:,1),'b')
hold on
errorbar(t(p+1:k+1),d(:,5),d(:,1),d(:,1),'r')
```

```
ylabel('Line width [mT]')
xlabel('Time [s]')

disp('')
disp('Please press any key.')
pause

bx=[p,k,p,k]
DAA=['Enter the start and stop of the mean [start,stop,start,stop] [',num
disp(DAA); aj=input(''); if isempty(aj); aj=bx; end
bx=aj;

bll=mean(d(bx(1)-p+1:bx(2)-p+1,5)), bstd=std(d(bx(1)-p+1:bx(2)-p+1,5))
bll1=mean(d(bx(3)-p+1:bx(4)-p+1,5));
bstd1=std(d(bx(3)-p+1:bx(4)-p+1,5));

clf;
plot(t,ytt(mmm,:),'g-')
ylabel('ESR Intensity [a.u.]; Line width [mT]')
xlabel('Time [s]')
title(idf)
hold on
plot(t(p+1:k+1),d(:,5),'b*',t(p+1:k+1),d(:,5),'r*')
plot(t(bx(1)+1:bx(2)+1),d(bx(1)-p+1:bx(2)-p+1,5),'go')
plot(t(bx(3)+1:bx(4)+1),d(bx(3)-p+1:bx(4)-p+1,5),'mo')

z=axis;
ytex=z(3)+0.4*(z(4)-z(3));
ysp=0.09*(z(4)-z(3));
xtex=z(1)+0.1*(z(2)-z(1));
ytex=ytex-ysp; DSP=['Broad line = ',num2str(bll),' [mT]'];
text(xtex,ytex,DSP);
ytex=ytex-ysp; DSP=['Linewidth = ',num2str(bll1),' [mT]'];
text(xtex,ytex,DSP);

save temp d
end
```

Bibliography

[1] Photocurable adhesive used for contacting transparent disk substrate and hub. 19941215. **1996**.

[2] Jahn, R.; Jung, T. *International Conference in Organic Coatings: Waterborne, High Solids, Powder Coatings, Proceedings, 26th, Athens, Greece, July 3-7, 2000* **2000**, pages 139–148.

[3] Batchelor, S. N.; Fischer, H. *J. Phys. Chem.* **1996**, *100*, 9794.

[4] Jahn, R.; Jung, T. *Progress in Organic Coatings* **2001**, *43*(1-3), 50–55.

[5] Baxter, J. E.; Davidson, R. S.; Hageman, H. J.; McLauchlan, K.; Stevens, D. G. **1987**, page 73.

[6] Borer, A.; Kirchmayr, R.; Rist, G. *HelV. Chim. Acta* **1978**, *61*, 305.

[7] Colley, C. S.; Grills, D. C.; Besley, N. A.; Jockusch, S.; Matousek, P.; Parker, A. W.; Towrie, M.; Turro, N. J.; Gill, P. M. W.; George, M. W. *J. Am. Chem. Soc.* **2002**, *124*, 14952.

[8] Dietliker, K.; Leppard, D.; Kunz, M.; Gatlik, I.; Kolczak, U.; Rzadek, P.; Rist, G. *The Spectrum* **1997**, *10*(3), 13.

[9] Mixture of photoinitiators. 19910228. **1991**.

[10] Pigmented photocurable composition. 19990224. **1999**.

[11] Dental material on the basis of hydroxyalkyl acrylamides. 20030620. **2004**.

[12] Curable coating composition containing uv-absorber acylphosphinoxide and hydroxy ketone photoinitiator. 20021121. **2003**.

[13] Gaze, C.; Gilbert, B. C. *J. Chem. Soc., Perkin Trans. 2* **1977**, (116).

[14] Gerson, F.; Gescheidt, G.; Knobel, J.; Martin, W. B.; Neumann, L.; Vogel, E. *J. Am. Chem. Soc.* **1992**, *114*, 7107.

[15] Gescheidt, G.; Lamprecht, A.; Ruechardt, C.; Schmittel, M. *HelV. Chim. Acta* **1991**, *74*, 2094.

[16] Hore, P. H.; Joslin, C. G.; McLauchlan, K. A. I. *Chemically Induced Dynamic Electron Polarization in Electron Spin Resonance*, Vol. 5 of *Specialist Periodical Reports;* Burlington House: London, 1979.

[17] Valet, A. *Progress in Organic Coatings* **1999**, *35*(1-4), 223–233.

[18] Photopolymerizable dental compositions. 19891228. **1991**.

[19] Jacobi, M.; Henne, A. *Polym. Paint Colour J.* **1985**, *175*, 636.

[20] Jokusch, S.; Turro, N. J. *J. Am. Chem. Soc.* **1998**, *120*, 11773.

[21] Jung, T.; Koehler, M.; Wostrazky, D. *SAMPE J.* **1998**, *34*(4), 40.

[22] Kolczak, U.; Rist, G.; Dietliker, K.; Wirz, J. *J. Am Chem. Soc.* **1996**, *118*, 6477.

[23] McLauchlan, K. A.; Simpson, N. J. K. *J. Chem. Soc., Perkin Trans. 2* **1990**, page 1371.

[24] Nelsen, S. F.; Ismagilov, R. F.; Powell, D. R. *J. Am. Chem. Soc.* **1997**, *119*, 10213.

[25] Norman, R. O. C. *Chem. Br.* **1970**, *66*, 6.

[26] Pedersen, J. B. *Theories of Chemically Induced Magnetic Polarization;* Odense University Press: Odense, Denmark, 1979.

[27] Pople, J. A.; Beveridge, D. L.; Dobosh, P. A. *J. Am. Chem. Soc.* **1968**, *90*, 4210.

[28] Rutsch, W.; Dietliker, K.; Leppard, D.; Koehler, M.; Misev, L.; Kolczak, U.; Rist, G. *Prog. Org. Coatings* **1996**, *27*, 227.

[29] Savitsky, A. N.; Paul, H. *Appl. Magn. Reson.* **1997**, *12*, 449.

[30] Slugett, G. W.; McGarry, P. F.; Koptyug, I. V.; Turro, N. J. *J. Am.Chem. Soc.* **1996**, *118*, 7367.

[31] Slugett, G. W.; Turro, C.; George, M. W.; Koptyug, I. V.; Turro, N. J. *J. Am. Chem. Soc.* **1995**, *117*, 5148.

[32] Sumiyoshi, T.; Schnabel, W. *Makromol. Chem.* **1985**, *186*, 1811.

[33] Verma, N. C.; Fessenden, R. W. *J. Chem. Phys.* **1973**, *58*, 2501.

[34] Turro, N. J. *J. Modern Molecular Photochemistry;* University Science Books:: Sausalito, CA,, 1991.

[35] Khudyakov, I. V.; Legg, J. C.; Purvis, M. B.; Overton, B. J. *Industrial and Engineering Chemistry Research* **1999**, *38*, 3353.

[36] Rist, G.; Borer, A.; Dietliker, K.; Desobry, V.; Fouassier, J. P.; Ruhlmann, D. *Macromolecules* **1992**, *25*(4182).

[37] Muller, U.; Aguirre, S. *J. Prakt. Chem.-Chem. Ztg.* **1992**, *334*, 603.

[38] Jockusch, S.; Turro, N. J. *J. Am. Chem. Soc.* **1999**, *121*, 3921.

[39] Leopold, D.; Fischer, H. *J. Chem. Soc.-Perkin Trans. 2* **1992**, page 513.

[40] Weber, M.; Khudyakov, I. V.; Turro, N. J. *J. Phys. Chem.* **2002**, *106*, 1938.

[41] Gatlik, I.; Rzadek, P.; Gescheidt, G.; Rist, G.; Hellrung, B.; Wirz, J.; Dietliker, K.; Hug, G.; Kunz, M.; Wolf, J.-P. *J. Am. Chem. Soc.* **1999**, *121*, 8332.

[42] Neville, A. G.; Brown, C. E.; Rayner, D. M.; Lusztyk, J.; Ingold, K. U. *J. Am. Chem. Soc.* **1991**, *113*, 1869.

[43] Brown, C. E.; Neville, A. G.; Rayner, D. M.; Ingold, K. U.; Lusztyk, J. *Aust. J. Chem.* **1995**, *48*, 363.

[44] Savitsky, A. N.; Galander, M.; Mbius, K. *Chem. Phys. Lett.* **2001**, *340*, 458.

[45] Geimer, J.; Beckert, D.; Jenichen, A. *Chem. Phys. Lett.* **1997**, *280*, 353.

[46] Vacek, K.; Geimer, J.; Beckert, D.; Mehnert, R. *J. Chem. Soc., Perkin Trans. 2* **1999**, page 2469.

[47] Prisner, T. F.; Rohrer, M.; Mbius, K. *Appl. Magn. Reson.* **1994**, *167*, 7.

[48] Fuhs, M.; Elger, G.; Osintsev, A.; Popov, A.; Kurreck, H.; Mbius, K. *Mol. Phys.* **2000**, *98*, 1025.

[49] Tsentalovich, Y. P.; Forbes, M. D. E. *Mol. Phys.* **2002**, *100*, 1209.

[50] Adrian, F. J.; Monchick, L. *J. Chem. Phys.* **1979**, *71*, 2600.

[51] Kaptein, R.; Oosterhoff, L. J. *Chem. Phys. Lett.* **1969**, *4*, 195.

[52] Pryor, W. A.; Smith, K. *J. Amer. Chem. Soc.* **1970**, *92*, 5403.

[53] Kawai, A. *Applied Magnetic Resonance* **2003**, *23*(3-4), 349–367.

[54] Murai, H.; Hayashi, H. *Radiation Curing in Polymer Science and Technology* **1993**, *2*, 63–154.

[55] Shushin, A. I.; Batchelor, S. N. *Journal of Chemical Physics* **2000**, *113*(14), 5873–5878.

[56] Shushin, A. I.; Pedersen, J. B.; Lolle, L. I. *Chemical Physics* **1993**, *177*(1), 119–31.

[57] Van Willigen, H.; Levstein, P. R.; Ebersole, M. H. *Magn. Reson.* **1991**, pages 333–51.

[58] Xu, X.; Zhang, X.; Cui, Z.; Lu, T. *Chemical Physics Letters* **2003**, *369*(5,6), 579–583.

[59] Goudsmit, G. H.; Paul, H.; Shushin, A. I. *Journal of Physical Chemistry* **1993**, *97*(50), 13243–9.

Chapter 8

Summary

The presented work has demonstrated, that TR-EPR is a powerful tool for the determination of the decisive structural and kinetic parameters for the evaluation of photoinitiator efficiency. Additional insights are provided by the application of theoretical calculations. This combination of experimental and theoretical methodology provides a basis for the design and development of innovative phototriggers.

On the bases of the results presented in this thesis we can make the following conclusions:

- TR-EPR allows the determination of addition rate constants in the cases where optical spectroscopy doesn't have sufficient resolution as well as provides structural information of the reactive species.

- Phosphinoyl radicals generated by photolysis of acyl and bis(acyl)phosphine oxides, possess high rate constants of addition to n-butyl acrylate, HDDA, styrene and 1-vynil-2-pyrrolidon. Analysis of the spin population at the phosphorus atom supports the experimental observations of TR-EPR spectra that greater localization of the spin population at the phosphorus atom results in faster rates of addition.

- A series of substituted benzoyl radicals have been generated by laser flash photolysis of α-amino ketones and bis(acyl)phosphine oxides. The benzoyl radicals were characterized by time-resolved EPR in toluene solution and their absolute rate constants for addition to n-butyl acrylate were determined. The experiments demonstrate two concentration domains of reactivity. The reactivity of benzoyl radicals decreases at high viscosity.

- Benzoyl radicals react faster with oxygen than phosphinoyl radicals, therefore, they can be used as oxygen scavenges.

- The fluorescence properties of the photoinitiators can be used to increase the in depth cure of the formulation.

- DFT and *ab initio* calculations have shown to be in a good agreement with the experimental data.

Curriculum Vitae

Address for Correspondence

Daniela Kirilova Hristova
Institute for Physical and Theoretical Chemistry
Graz University of Technology
Technikerstraße 4/I
A-8010 Graz

Tel. +43 316 8738733
Fax +43 316 8738225

hristova@ptc.tugraz.at

Education

July 2003 - now,	Continuation of the PhD study in the Institute for Physical and Theoretical Chemistry, Graz University of Technology, Austria (The group moved from the University of Basel to the Graz University of Technology)
Nov. 2001 - July 2003,	Beginning of the PhD study in the Department of Chemistry, University of Basel, Switzerland
May. 2001 – Sept. 2001,	Master thesis in the Institute of Medical Chemistry (C.S.I.C.), Madrid, Spain
Sept. 1996 – Nov. 2001,	University of Chemical Technology and Metallurgy, Sofia, Bulgaria MS degree in "Technology of Organic synthesis", Qualification: Chemical engineer
Sept. 1991 – July 1996,	High school, English Language School "Petar Beron", Kjustendil, Bulgaria

Experience

Nov. 2001 – now	Ph.D. student in the University of Basel and Graz University of Technology.

- TR-ESR, CW-ESR, fluorescence spectroscopy and computational methods.

- Determination of the addition rate constant for a variety of phosphorus and carbon centered radicals

to the double bond of different monomers, as well as their reaction with molecular oxygen.

- Fluorescence measurement of different photoinitiators for radical polymerization
- Theoretical calculations with the Gaussian Package using different levels of theory (HF, DFT, MP2, MP4,G2,G3) to obtain equilibrium and transition state structures, hyperfine coupling constants, schematic potential energy profiles, single point energies (including CBS and BSSE calculations), thermochemical quantities such as the reaction barrier and exothermicity.

May 2001- Sept. 2001	Instituto de Química Médica (C.S.I.C.), Madrid, Spain, Lab. of Organic Synthesis.

- Synthesis and investigations on heterocyclic compounds with antiviral and antitumor activity.
- Chemistry of quinones, covering mechanistic and synthetic aspects.
- epoxides as precursors for the compounds with antitumor activities

April 1998 – April 2000	University of Chemical Technology and Metallurgy, Sofia Laboratory of IR spectroscopy, HPLC and GC-MS analysis, International project between "University of Chemical Technology and Metallurgy", Sofia and "Instituto de Química Médica", Madrid, Spain "Synthesis and application of 1,4- and 9,10-anthraquinones"
Summer 1999	"Industrial synthesis of analgesics", Sopharma, Bulgaria
Summer 2000	"Industrial synthesis of Neuroleptics", Sopharma, Bulgaria

Fellowships

- **Ph.D.** fellowship from Ciba Research Foundation, Basel, Switzerland (2001-now)
- **ERASMUS** fellowship for 5 months stay in the Organic Synthesis group, Instituto de Química Médica (C.S.I.C.), Madrid, Spain

Skills

- Synthesis of organic compounds in the scale from 1 mg to 1 kg.
- Characterization of organic compounds: NMR (^{1}H, ^{13}C, COSY, HSQC, HMBC), FTIR, HPLC, GC-MS, MS, UV-VIS, CW-ESR, Fluorescence spectroscopy
- Time-resolved measurements

- TR-ESR
- Single photon counting
- Application of quantum chemical programs
- Languages:
  - Bulgarian – native language
  - English – excellent
  - German – very good
  - Spanish – average
  - Russian – very good

Hobbies

- Hobbies are gradually moving from reading and listening music to enjoying good cooking
- Sport activities like skiing, biking, swimming, hiking and badminton
- Traveling

Participation in Conferences and Publications

1. Daniela Hristova, Iwo Gatlik, Georg Gescheidt, Günther Rist, Kurt Dietliker, Jean-Pierre Wolf, Jean-Luc Birbaum, Anton Savitsky, and Klaus Möbius, *Addition of Benzoyl Radicals to Butyl Acrylate: Absolute Rate Constants by TR-EPR*, Macromolecules, (in press)

2. Kurt Dietliker, Tunja Jung, Johannes Benkhoff, Hisatoshi Kura, Akira Matsumoto, Hidetaka Oka, Daniela Hristova, Georg Gescheidt, Günther Rist, *New Developments in Photoinitiators*, Macromol. Symp. 2004, 217,77-97

3. Daniela Hristova, Iwo Gatlik, Georg Gescheidt, Günther Rist, Kurt Dietliker, Jean-Pierre Wolf, Jean-Luc Birbaum, Anton Savitsky, and Klaus Möbius, *Addition of Benzoyl Radicals to Butyl Acrylate: Absolute Rate Constants by TR-EPR*, 37th Annual International Meeting Electron Spin Resonance Group of the Royal Society of Chemistry, March 28th – April 1st, 2004, Warwick, UK

4. Iwo Gatlik, Daniela Hristova, Georg Gescheidt, Günther Rist, Kurt Dietliker, Jean-Pierre Wolf, Jean-Luc Birbaum, Anton Savitsky, and Klaus Möbius , *Viscosity Dependence of Radical reactivity*, Workshop on Radical Ion Reactivity in Biology, Chemistry and Technology, June 16th – 21st, 2002, Heigenbrücken, Germany.

5. Tz.Philipova, M.T.Molina, D.Hristova, *New Dispersed and Structurally colored polymers with 1,4-Anthraquinones*, 2nd International Conference on Chemical Sciences for Sustainable Development, June 6th – 9th, 2000, Halkidiki, Greece.

During my education at the University of Basel and Graz University of Technology I attended the lectures and courses of the following professors and lecturers:

Prof. Georg Gescheidt, Prof. B. Giese, Prof. J. Wirz, Prof. H. Huber, Prof. A. Vedani, Prof. J. Seeliq
at the University of Basel

Prof. G. Grampp, Prof. K. Gatterer, Prof. G. Gescheidt, Dr. Anne-Marie Kelterer, Dr. S. Landgraf, Prof. M. Ramek
at the Technical University of Graz